IEEE Access
Multidisciplinary | Rapid Review | Open Access Journal

Received January 19, 2020, accepted February 17, 2020, date of publication March 2, 2020, date of current version March 13, 2020.

Digital Object Identifier 10.1109/ACCESS.2020.2977690

Automatic Infrared Ship Target Segmentation Based on Structure Tensor and Maximum Histogram Entropy

YONGSONG LI[1,2], ZHENGZHOU LI[1,2,3], ZHIQUAN DING[4], TIANQI QIN[4], AND WEIQI XIONG[1,2]

[1]School of Microelectronics and Communication Engineering, Chongqing University, Chongqing 400044, China
[2]Key Laboratory of Dependable Service Computing in Cyber Physical Society of Ministry of Education, Chongqing University, Chongqing 400044, China
[3]Key Laboratory of Optical Engineering, Institute of Optics and Electronics, Chinese Academy of Sciences, Chengdu 610209, China
[4]Sichuan Institute of Aerospace Electronic Equipment, Chengdu 610100, China

Corresponding author: Zhengzhou Li (lizhengzhou@cqu.edu.cn)

This work was supported in part by the National Natural Science Foundation of China under Grant 61675036, in part by the Chinese Academy of Sciences Key Laboratory of Beam Control Fund under Grant 2017LBC006, and in part by the 13th Five-year Plan Equipment Pre-Research Fund.

ABSTRACT The existing infrared (IR) ship target segmentation methods may suffer serious performance degradation in the situation of diverse background clutters and ship targets. To cope with this problem, a novel ship target segmentation method is proposed in this paper. Initially, the IR image is transformed into the map of large eigenvalues of structure tensor (STLE), where the horizon line and ship target boundary can be explicitly characterized. According to the scene context clue, the automatic horizon line detection (AHLD) is proposed to efficiently judge the existence of horizon line and remove sky/land region clutters. Then, based on the intensity distribution of ship target and sea background, the adaptive maximum histogram entropy (AMHE) is presented to accurately perceive the brightness (dark or bright) of ship target, and coarsely segment the bright or dark ship target from sea background. After that, considering the ship target boundary information, the regions-of-interest (ROI) of ship target is located and the ship foreground map (SFM) is developed to address the under-segmentation. Finally, a new Watershed algorithm namely structure tensor and maximum histogram entropy modified Watershed transform (TEWT) is constructed to completely extract the whole ship target. Extensive experiments show that the proposed method outperforms the state-of-the-art methods, especially for IR images with intricate background clutter and heavy noise. Moreover, the proposed method can work stably for ship target with unknown brightness, uneven intensities, low contrast, variable quantities, sizes, and shapes.

INDEX TERMS Infrared (IR) imaging, ship target segmentation, structure tensor, maximum histogram entropy, modified watershed transform.

I. INTRODUCTION

Automatic ship target segmentation is an important issue for maritime infrared search and track (IRST) systems, such as maritime rescue, traffic monitoring and coastal defense, where both accuracy and robustness are indispensable [1]–[3]. However, because infrared imaging depends on weather conditions, sea surface reflections and thermal radiations between ship target and background, the infrared ship images are vulnerable to changeable imaging scenarios and can be characterized by low signal-to-noise ratio (SNR), low signal-to-clutter ratio (SCR) and lack of details. Therefore, infrared ship target segmentation is still considered as a challenging work [4]–[6].

Although many researchers have made a lot of effort for infrared ship target segmentation and proposed numerous corresponding methods, there are still the following main downsides, which make it difficult to achieve robust segmentation and limit their practical applications:

1) In general, the diverse background clutters especially sky/land region clutters (e.g. buildings, cars, clouds and islands) in IR ship image are unpredictable. Therefore, the regular ship target segmentation method [2], [7] processes the whole IR image regardless of the scene information,

The associate editor coordinating the review of this manuscript and approving it for publication was Shuo Sun.

This work is licensed under a Creative Commons Attribution 4.0 License. For more information, see http://creativecommons.org/licenses/by/4.0/

which will be seriously disturbed by the sky/land region clutters. As an important scene context information for maritime target detection and segmentation, horizon line (i.e. sea-sky-line/coastline) can provide the region division clue to remove the disturbance of sky/land region clutters and validate the real ship targets. Thereby, some researches directly located the longest straight line in the edge map as the horizon line to eliminate the sky/land region clutters [3]. However, because IR ship image itself has a lot of noise and sea clutter, classical edge detectors [6], [13] will detect a large of tiny and trivial noise edges and cannot depict the real horizon line. Moreover, since the pitch angle between the imaging platform and the sea level is variable and whether the horizon line exists is unknown, the above two rude processing approaches will reduce the accuracy of IR ship target segmentation under diverse backgrounds.

2) Previous studies [1], [9], [15], [23] mostly focus on the bright IR ship target segmentation, but the dark target whose IR radiation is lower than sea background also exist in the backlighting IR images but is seldom covered. Hence, these methods cannot extract the IR dark ship target from the brighter maritime background. Nevertheless, in the real-world IR maritime scenes, the global-contrast brightness (bright or dark) of ship target is unknown [15], so adaptive ship target segmentation for both bright and dark ones in IR image remains to be worthy of further investigation.

3) Even in the sea region, the background clutter may also have some uneven areas whose gray-level intensity is close to the ship target (e.g. tail wave, reflective clutter and backlit clutter). Accordingly, the intensity-based ship target segmentation methods [10], [12], [16] will introduce those uneven parts into the segmentation result and cause under-segmentation. Furthermore, by staring at the appearance model of ship target in IR image, the existing methods commonly assume that the ship target is the uniform region against the sea background [22], [25], [26]. However, for IR ship image with low contrast or near-distance imaging, the intensity of ship target will be inhomogeneous and even the inner parts of the ship target with strong opposite intensities. Therefore, these methods can easily lose the uneven parts of ship target, resulting in over-segmentation. In summary, under-segmentation and over-segmentation are two well-known difficulties for existing IR ship target segmentation methods, which need more in-depth research.

4) The algorithm for IRST applications will be implemented on common embedded system with limited computing resources in the future, thus it should meet the potential demand of real-time computation.

To address the above drawbacks, this paper proposes an effective and robust ship segmentation scheme based on structure tensor and maximum histogram entropy (MHE) [38] according to the intrinsic IR imaging characteristics between ship target and background clutter. Firstly, the IR image is transformed into the map of large eigenvalues of structure tensor (STLE), where the horizon line and ship target boundary can be explicitly depicted. According to the scene context clue of IR ship image, the automatic horizon line detection (AHLD) is proposed to judge whether the horizon line exists and remove the sky/land region clutters. Then, according to the intensity distribution of IR ship target and sea background, the adaptive MHE (AMHE) is presented to perceive the brightness (dark or bright) of ship target, and segment the ship target from sea background, but may cause under- or over-segmentation. Finally, to overcome those two problems, considering the boundary information of IR ship target, a two-step strategy is introduced to refine the ship target segmentation by reasonably incorporating the boundary information into the AMHE segmentation results. Extensive experiments show that the proposed IR ship target segmentation scheme outperforms the compared existing algorithms under diverse backgrounds and heavy noise, and is suitable for ship targets with unknown brightness, uneven intensities and variable quantities, sizes, and shapes.

There are four contributions in this paper:

1) The STLE is introduced to perceive the thick and rough edge characters of IR ship images while ignoring the small and trivial details, so the horizon line and ship target boundary can be well delineated. In addition, the AHLD is proposed to automatically determine the existence of horizon line and locate the horizon line, so the sky or land region clutters can be reliably removed.

2) The AMHE is presented to accurately perceive the brightness (bright or dark) of IR ship target, and adaptively segment the bright or dark ship target from sea background. Meanwhile, the MHE guided gray-level morphological reconstruction (EGMR) is designed to adaptively smooth intricate sea clutters and heavy noise, and drive the brightness and intensity of ship target to be more consistent, so that the boundary information of the ship target can be more reliably incorporated into the segmentation refinement procedure.

3) By using the edge strength-based patch selection method in the binary STLE map to locate the regions-of-interest (ROI) of ship target, the ship foreground map (SFM) is developed to efficiently eliminate the sea clutter regions whose gray-level intensity is approximate to the ship target and conquer the under-segmentation deficiency. Furthermore, by fully integrating the both advantages of STLE and MHE, a new Watershed algorithm named as structure tensor and maximum histogram entropy modified Watershed transform (TEWT) is constructed to completely segment the IR ship target with extremely uneven intensities.

4) Combining above methods and their advantages, an efficient and robust infrared ship segmentation scheme is developed and is superior to the compared state-of-the-art ship target segmentation methods. Moreover, the proposed method is computationally economical and has the potential for real-time applications.

The structure of this paper is organized as follows: Section II reviews the related works on IR ship target segmentation. The signature characters of ship target and background clutter in IR image are described in Section III. The efficiency

of STLE is discussed and the AHLD for removing sky/land clutters is proposed in the Section IV. In Section V, the AMHE is presented to adaptively segment bright or dark ship target from sea background. The two-step refinement for ship target segmentation is developed in Section VI. Extensive experiments are included in Section VII to evaluate the performance of the proposed method. Finally, Section VIII gives the conclusions of this paper.

II. RELATED WORK

Many infrared ship target segmentation algorithms have been developed in recent years, which can be roughly divided into four categories: background modeling-based methods, thresholding-based methods, active contour-based methods, and feature analysis-based methods.

In the background modeling-based methods, the background pixels are assumed to obey a certain probability density function (PDF), while the ship target is regarded as an abnormal component with great contrast. In [7], the regions-of-interests are firstly located by variance weighted information entropy and the background is molded by Gaussian Markov random field (MRF), then the infrared target regions are extracted by background subtraction. In [8], the infrared image is divided into a set of image blocks and the radiation anomaly of each block is calculated by Gaussian mixture model (GMM), then the ship target is checked by a discriminative criterion in the anomaly image blocks. Recently, Zhou *et al.* [9] developed a high order statistic filtering in fractional Fourier domain to predict the background, and the ship component is detected by the maximal peak interval in the high order statistic curve. These background modeling-based methods have outstanding performance for common static maritime background suppression. However, for infrared image with non-stationary complex background clutters, simply treating the background as a pre-supposed PDF is incorrect and will reduce the ship segmentation performance.

In the thresholding-based methods, each pixel of infrared image is considered as two-class (background class and ship target class) division problem and is discriminated with an optimal threshold by fully considering the gray intensity distribution of infrared ship image. The well-known two-dimensional (2-D) Otsu [10] and 2-D maximum entropy [11], [12] were used to find the optimal segmentation threshold by transferring the IR ship image into the 2-D histogram. Zhang and Wu *et al.* [13], [14] employed Canny operator to locate sea-sky line, and presented a recursive Otsu segmentation method including global Otsu and local Otsu to extract ship targets. Lately, Wang *et al.* [15] reported an adaptive threshold segmentation method based on gray histogram curve transform. By cyclically shifting the image histogram, the average gray level could be the optimal threshold for detecting targets. Yin *et al.* [16] proposed an IR ship segmentation scheme based on fuzzy correlation and graph cut optimization. The fuzzy correlation model constructed by the S-shape function is used to search the optimal threshold and the graph cut optimization is performed on the infrared image for achieving completed segmentation result. Those thresholding-based methods are widely used in the field of ship target segmentation for their simplicity and easy-implementation. Nevertheless, those methods only take the gray intensity information into account, but less consider the local spatial information and context information. Therefore, the thresholding-based methods cannot extract real ship targets, when the gray level of sea clutters is close to that of ships or the ship target and background are heterogeneous.

The active contour-based methods are based on the curve evolution and convex optimization of a given energy function to segment ship targets. In the early active contour-based methods, Szpak and Tapamo [17] adopted a background subtraction method to detect moving ship targets and used the level set-based active contour model to segment and track the moving targets in the ocean. To further improve the accuracy of Szpak's level set method, Frost and Tapamo [18] integrated the ship prior-known shape information into the energy functional for ship segmentation. Furthermore, Fang *et al.* appended boundary information [19] and local entropy energy [20] into the level set model to improve the segmentation performance of ship targets with relatively heterogeneous intensity. These active contour-based methods work well for ship target with relatively uneven intensity and weak boundary to some extent. Whereas, the ship targets cannot be segmented from the chaotic sea clutters with non-negligible topology information. In addition, the segmentation performance of these methods is easily affected by initial contour, iterations and time consumption. These limitations decline their application in practical ship target detection.

The feature analysis-based methods have been drawing more and more attention in the past several years. In the study of Tao *et al.* [21], the infrared image is filtered by mean-shift algorithm based on gray feature space to form divided regions, and then the divided regions are processed by a graph region merging procedure to obtain the final segmented ship target. The method can efficiently segment the ship object under the disturbance of sea clutter. However, because the method is based on region merging, when the ship target is too large or low contrast, the target will be wrongly merged with the background. Liu *et al.* [22] presented a multi-feature integration (MFI) method, which includes gray intensity feature for segmenting potential target regions and four shape features for identifying ship targets. By integrating more features of ship targets including local contrast, salient linear structure and edge strength, the segmentation performance of MFI method is further enhanced [23]. The MFI methods can efficiently segment ship targets in heterogeneous background due to the full consideration of the multiple features of ship targets. Nevertheless, these methods are based on the assumption that the target regions are relatively brighter than the dark sea surface, so they cannot detect the negative-contrast dark ship targets under relatively bright sea background. Bai *et al.* [1], [24] improved the classical fuzzy c-means (FCM) clustering by adding nonlocal spatial

information and the spatial shape information of the infrared ship target, which can efficiently segment the ship target in weakly textured backgrounds. In addition, the feature-based fuzzy inference system was suggested in [25] to segment infrared ship targets. In this system, the intensity feature, local spatial feature and global spatial feature are fuzzified using prior knowledge, and the ship targets are segmented and extracted by fuzzy inference. The method can effectively extract ship targets in low-contrast infrared images. Yet since the fuzzy inference system is based on prior knowledge, the uncertainty of ship segmentation results would be increased in complex and changeable sea clutter. In our previous work [26], we developed an IR ship target detection method based on morphological reconstruction and multi-feature analysis. Due to the reasonable integration of multiple features after gray-level morphological reconstruction, the method is robust to the detection of both bright and dark small ship target submerged in heavy sea clutter. However, the method is based on the assumption that ship targets are viewed as uniform regions under the sea background in long-distance IR imaging, so it cannot work well for segmenting the entire ship target with uneven intensities in near-distance imaging.

Comparing the advantages and disadvantages of above-mentioned methods, although many studies have been focused on the segmentation of IR ship target against complex background in the past decades, it is still an open issue. To further overcome the disturbance of heterogeneous background clutters and heavy noise on the segmentation of ship targets with unknown brightness, uneven intensities, low contrast and different sizes, an effective and robust ship segmentation scheme based on structure tensor and maximum histogram entropy (MHE) according to the intrinsic IR imaging characteristics between ship target and background clutter is proposed in this paper.

III. SIGNATURE CHARACTERS OF SHIP TARGET AND BACKGROUND CLUTTER IN INFRARED IMAGES

An IR ship image is commonly composed of three parts: ship target, background clutter and noise component, and can be briefly modeled as:

$$f(x, y) = f_{st}(x, y) + f_b(x, y) + f_n(x, y) \tag{1}$$

where $f(x, y), f_{st}(x, y), f_b(x, y)$ and $f_n(x, y)$ denote the original infrared image, the ship target image, the background clutter image, and the noise image at pixel location (x, y), respectively. In this paper, the noise f_n is deemed as an additive white Gaussian noise. Depending on the characters of f_{st}, or the characters of f_b or both of them, different ship target segmentation methods are designed in the past decades. Actually, in IR images, because different materials have different thermal radiations, and the hotter object appears ''white'' while the cooler object appears ''black'', the ship target as manmade objects in sea clutter can naturally form bright or dark regions in the IR image despite the ship camouflage colors and the illumination condition in visible images.

FIGURE 1. Samples of infrared ship target images.

However, IR imaging results are complex and comprehensive processes, which are easily affected by non-stationary inputs, such as atmospheric radiations, solar refractions and engine temperatures. Therefore, the characters of IR ship images are usually various and unpredictable [26], [27].

Nevertheless, it can be seen from Fig. 1 that although different IR images have different ship targets and background clutters, they still have some common points. Generally, there are mainly three regions in IR ship images: sky/land, ship target and sea background, and the three regions have some certain distinguishable clues and properties. Through the observation of the IR ship images, we find that there are following three common properties and corresponding difficulties:

Property 1: The horizon line (sea-sky-line/coastline) is a thick and rough edge, which can be used as the cue to remove the sky/land region clutters (such as buildings, cars, clouds and islands), but it is often weak and has some discontinuous and warping parts.

Property 2: The main body of ship target is much smaller than sea background, and they have different gray-level intensity features, but their intensities are inhomogeneous and brightness (relative bright or dark) are unknown.

Property 3: The boundary of ship target is more conspicuous than its surroundings and sea background, but how to reasonably delineate and incorporate it to refine the ship target segmentation is a problem to be solved.

Depending on the above three properties and difficulties, we develop an automatic IR ship target segmentation scheme in this paper based on structure tensor and maximum histogram entropy (MHE). Firstly, the IR image is transformed into the STLE map, where the thick and rough edge characters of horizon line and ship target boundary can be well depicted. Hence, according to ***Property 1***, the AHLD method based on binary STLE (BSTLE) and Hough transform is proposed to efficiently judge whether the horizon line exists and remove the sky/land region clutters. Then, according to ***Property 2***, the AMHE is presented to accurately detect the ship hull brightness (relative dark or bright) and automatically segment the main body of ship target from sea background. However, the segmentation results of AMHE are relatively coarse, and may cause some under- or over-segmentation phenomena. To address those two problems, we introduce a two-step strategy to refine the IR ship target segmentation by reasonably incorporating the boundary information of

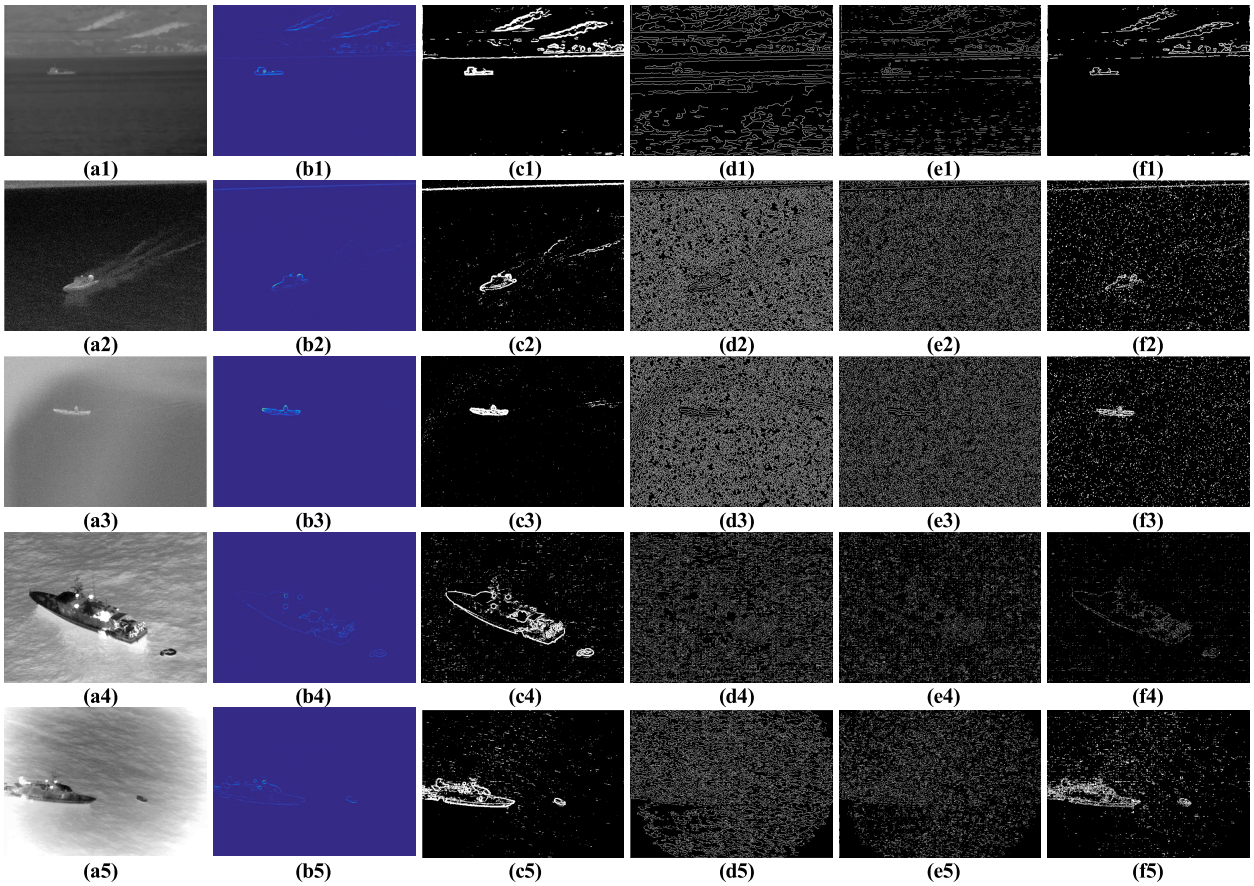

FIGURE 2. Comparison results of different edge detectors on five representative IR ship images. (a) original IR ship images. (b) The STLE map shown by color map. (c) The edge map computed by designed BSTLE. (d) The edge map computed Canny detector. (e) The edge map computed by LoG operator. (f) The edge map computed by adaptive Canny detector.

ship target (according to ***Property 3***). In order to make the use of boundary information more reliable, the EGMR filter is designed to adaptively smooth heavy noise clutters and drive the brightness and intensity of ship target to be more consistent. Thereby, after EGMR filtering, the recomputed STLE (rSTLE) and recomputed BSTLE (rBSTLE) can be obtained to reliably correct the boundary information of ship target. After that, according to the boundary information of ship target, the rBSTLE-based edge image patches selection method is proposed to locate the ROI of ship target and then the SFM is developed to address the under-segmentation. Finally, the SFM and the complement of the ROI map are extracted as the marker image, and the rSTLE map is imposed to the minima by the extracted marker image to obtain the final rectified boundary information (FRBI) of ship target. By taking the FRBI of ship target as the watershed line, the TEWT is constructed to efficiently extract the entire ship target. The details of the proposed method will be introduced in the following sections.

IV. AUTOMATIC HORIZON LINE DETECTION FOR SKY/LAND REGION CLUTTER REMOVAL

A. LARGE EIGENVALUES OF STRUCTURE TENSOR

According to the ***Property 1*** and ***Property 3*** of IR ship images, both the horizon line and ship target boundary have obvious thick and rough edge characters. Therefore, given the original IR image f, the corresponding local gradient ∇f can be firstly computed to describe the edge characters:

$$\nabla f(x, y) = \left[\frac{\partial f}{\partial x}, \frac{\partial f}{\partial y}\right] \tag{2}$$

$$\frac{\partial f}{\partial x} = \frac{f(x+1, y) - f(x-1, y)}{2} \tag{3}$$

$$\frac{\partial f}{\partial y} = \frac{f(x, y+1) - f(x, y-1)}{2} \tag{4}$$

where $\partial f / \partial x$ and $\partial f / \partial y$ are the partial derivative value in x direction and y direction, respectively. Because the conventional local gradient detector (as Canny detector in Fig. 2(d1-d5)) only considers the local pixel differences and does not estimate the local image structure, it is easily affected by noise and trivial clutters, resulting in the actual thick and rough edges not being well perceived. Recently, the structure tensor as a powerful tool for locally structural information analysis has achieved some impressive results [28]–[30]. This is because the structure tensor is able to transform the original relationship of the gradient in the image into a new structure relationship, which is more effective for the perceptivity on the dominant edge at the local image. In light of this finding, we use the structure tensor

to perceive the thick and rough edge characters. Given a 2-D discrete image f, the structure tensor ST of image f is calculated as:

$$\begin{aligned} ST(x,y) &= G_\sigma(x,y) \otimes \left\{ \nabla f(x,y) \times [\nabla f(x,y)]^T \right\} \\ &= G_\sigma(x,y) \otimes \begin{bmatrix} \left(\frac{\partial f}{\partial x}\right)^2 & \frac{\partial^2 f}{\partial x \partial y} \\ \frac{\partial^2 f}{\partial x \partial y} & \left(\frac{\partial f}{\partial y}\right)^2 \end{bmatrix} = \begin{bmatrix} ST_{11} & ST_{12} \\ ST_{21} & ST_{22} \end{bmatrix} \end{aligned} \tag{5}$$

where $\otimes$ is the convolution operator, and the Gaussian kernel function $G_\sigma(x,y)$ is written as:

$$G_\sigma(x,y) = \frac{1}{2\pi\sigma^2} e^{-\frac{x^2+y^2}{2\sigma^2}} \tag{6}$$

The Gaussian kernel function can be considered as a window of ST to perceive the locally structural information and σ determines the size of the window. The σ is empirically set to 4. We have investigated the two eigenvalues of local matrix ST, and found that the large one can depict the thick and rough edges while ignoring the small and trivial details [26], but the small one mainly locates corners and has little contribution to the strong and thick edges. Hence, here we simply utilize the large eigenvalues of structure tensor (STLE) to depict the edge characters of horizon line and ship target boundary in IR image, and the STLE map λ_{large} can be expressed as:

$$\begin{aligned} &\lambda_{\text{large}}(x,y) \\ &= N\left[\frac{1}{2}\left(ST_{11} + ST_{22} + \sqrt{(ST_{11}-ST_{22})^2 + 4ST_{12}ST_{21}}\right)\right] \end{aligned} \tag{7}$$

where $N(\bullet)$ is the normalization function normalized into the range [0,1] by using maximum and minimum values. Because the STLE map can indicate the predominate direction and the coherence degree of the gradient strength, the horizon line and ship target boundary can be enhanced while the trivial clutters and noise can be suppressed, as Fig. 2(b1-b5) illustrates. After the calculation of STLE map, a simple but effective edge detector namely binary STLE (BSTLE) is designed, and the BSTLE can be derived as:

$$BSTLE(x,y) = \begin{cases} 1, & \lambda_{\text{large}}(x,y) \geq \tau \\ 0, & otherwise \end{cases} \tag{8}$$

here the adaptive threshold τ is determined as:

$$\tau = \overline{\lambda_{\text{large}}} + \varepsilon \times std(\lambda_{\text{large}}) \tag{9}$$

where $\overline{\lambda_{\text{large}}}$ and $std(\lambda_{\text{large}})$ are the mean value and standard deviation of the STLE map λ_{large}, respectively. ε is an experimentally selected constant and it can be chosen as 0.5 for most maritime scenarios.

To illustrate the efficiency and robustness of the BSTLE to delineate the thick and rough edge characters of the horizon line and ship target boundary, we conducted experiments on the five selected representative IR ship images with complex maritime scene clutters. The classical edge detectors, such as Canny detector [13], [14], Laplacian of Gaussian (LoG) operator [6], and adaptive Canny detector [31] are chosen as the compared methods, because they were commonly used as the edge descriptors for the horizon line and ship boundary. Fig. 2 shows the comparison results of different edge detectors on five representative IR ship images. The first IR image of Fig. 2 is a bright ship target disturbed by intricate land clutters but with weak coastline, and its image size is 640×480. The second IR image is a bright ship target corrupted by strong long-tail waves and heavy Gaussian noise (standard deviation is 20) in sea-sky background, and its image size is 640×480. The third IR image is the bright ship target interfered by the bright sea clutter region whose gray-level intensity is close to the ship target and Gaussian noise (standard deviation is 8), and its image size is 720×480. The fourth IR image is a huge and dark ship target with uneven intensities submerged in heavy sea clutters, and its image size is 1450×1107. The fifth IR image is a large and dark ship target with extremely uneven intensities, half of which is buried in inhomogeneous sea background, and its image size is 1024×775. Their aspect ratios are all shown as 4:3 in this paper for better display.

As can be seen from Fig. 2, the edge detection results of Canny detector and LoG operator both leave a large amount of false edges and eventually cannot detect the real edges of horizon line and ship target contour on all five IR ship images. They extract image edges by observing the changes of the first or second-order directional derivatives around each pixel neighborhood, but cannot consider the local image structure, thus being susceptible to trivial details. Because the IR ship image itself has a lot of noise and sea clutter, the Canny detector and LoG operator will detect these tiny and trivial edges, which eventually leads to the true thick and rough edges not being well characterized. By integrating the histogram equalization algorithm, the adaptive Canny detector is much better than above two algorithms and can roughly detect the edges of the ship target on Fig. 2 (a1) and (a3)-(a5). However, due to the use of histogram equalization algorithm, the weak thick and rough edges will be suppressed, and the adaptive Canny detector cannot detect the weak horizon line, as shown in Fig. 2(f1). Moreover, the adaptive Canny detector cannot well detect the ship target boundary when the image is corrupted by heavy noise and sea clutters, as shown in Fig. 2(f2)-(f5). As can be seen from Fig. 2(c), compared with Canny detector, LoG operator and adaptive Canny detector, the edge detection results of the BSTLE are better than those of the other three detectors, which can completely delineate all horizon lines and ship hull boundaries and has lower false edge residues. This robustness is attributed to the fact that the BSTLE can perceive local structure information by utilizing Gaussian kernel function in structure tensor, and can depict thick and rough edges while ignoring the trivial details by projecting this information into the map of large eigenvalues.

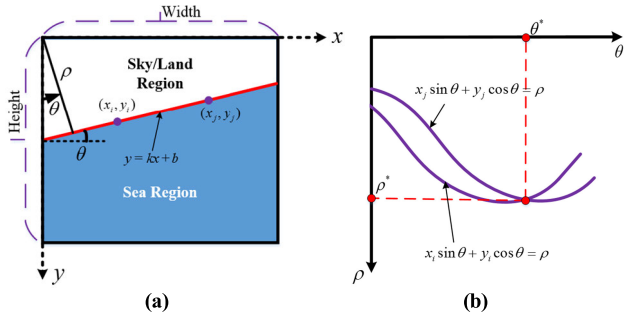

FIGURE 3. Illustration of Hough transform for horizon line extraction. (a) Parameters of a straight line in x-y coordinate system in the image domain; (b) Sine parametric curves of a straight line in θ-ρ coordinate system.

B. AUTOMATIC HORIZON LINE DETECTION (AHLD)

Horizon line is a very important scene context information for maritime target detection and segmentation [3], [14], [32], because it can provide the region division clue to remove the disturbance of sky/land region clutters (like clouds, buildings, cars and islands) and validate the real ship targets. For this reason, an automatic horizon line detection (AHLD) method based on BSTLE and Hough transform is proposed in the first step of segmentation to remove sky/land region clutters and reduce the search space for ship targets. As shown in Fig. 2(c1) and (c2), the thick and rough edge characters of horizon line can be well delineated by BSTLE, and the horizon line is approximately regarded as the longest thick straight line in the BSTLE map. Therefore, as Fig. 3(a) illustrates, the horizon line in BSTLE map can be briefly written as:

$$y = kx + b = \left(-\frac{\sin\theta}{\cos\theta}\right)x + \frac{\rho}{\cos\theta} \tag{10}$$

where k is the slope, b is the intercept of horizon line; θ is the angle between the horizon line's normal and y-axis, ρ is the distance between origin and horizon line. Firstly, each edge pixel with coordinates (x, y) in BSTLE map is transformed into a Sine parametric curve in the Hough space (θ, ρ) using the projection [3], [33]:

$$H(\theta, \rho) = \sum_{x=1}^{Width}\sum_{y=1}^{Height}(1 - \delta(BSTLE(x, y))) \times \delta(x\sin\theta + y\cos\theta - \rho) \tag{11}$$

where $\delta(\bullet)$ represents the Dirac delta function and $BSTLE(x, y)$ is the computed edge map. *Width* and *Height* represent the width and height of the IR image. This is analogous to computing the 2D curve intersection counting accumulators of (θ, ρ), as Fig. 3(b) shows. Accumulator cells in the θ-ρ plane corresponding to few largest values $H(\theta, \rho)$ determine the parameters of the several straight lines that pass through the most edge points. Because the horizon line can be well characterized in the BSTLE map and presents the longest thick straight line, we select the largest number $H^*(\theta^*, \rho^*)$ in the line set after Hough transform to determine the potential horizon line in the image.

Unfortunately, although Hough transform can reliably locate the longest line (i.e. the potential horizon line) in each BSTLE map, for practical maritime scenes, since the pitch angle between the infrared imaging platform and the sea level is variable, the existence of horizon line is unknown. To cope with problem, a standard metric γ to judge whether the horizon line exists or not is suggested as:

$$\gamma = \frac{H^* \times \cos\theta^*}{Width} \tag{12}$$

where H^* and θ^* denote the edge point number and angle computed by Hough transform of the potential horizon line, respectively. Therefore, the standard metric $\gamma(\gamma \in (0, 2))$ fully considers the length, slope and edge thickness of the detected line in the BSTLE map to determine whether it is the horizon line. Based on the statistics and observation of 90 different IR maritime scene images, the standard metric is empirically set as $\gamma = 0.7$ in our experiments. This means if the standard metric γ of the detected line is no less than 0.7, then the detected line is considered as the real horizon line, and meanwhile the pixel intensity of the region above the horizon line (sky or land region) will be set to 0, while the region below the horizon (sea region) will be totally preserved. Otherwise, the horizon line does not exist in the IR ship image, and the detected line will not be outputted, so the whole image will be regarded as the sea region and directly output to the next segmentation step. The whole of the proposed automatic horizon line detection (AHLD) algorithm for sky or land region clutters removal in IR ship image based on STLE and Hough transform is summarized in **Algorithm 1**.

The standard metrics γ of the detected line for Fig. 2(a1-a5) are 1.2718, 1.3395, 0.3437, 0.4098 and 0.4419, respectively. Therefore, through the calculation of the proposed AHLD method, the results of the final detected horizon line and the removal of the sky/land region for Fig. 2(a1) and (a2) are shown in Fig. 4. No horizon line is detected for Fig. 2(a3)-(a5), so the original IR ship images are entirely output to the next processing step.

V. ADAPTIVE MAXIMUM HISTOGRAM ENTROPY FOR SHIP TARGET BRIGHTNESS PERCEPTION AND SEGMENTATION

As can be seen from Fig. 2 and Fig. 4, the sky/land region clutters can be removed completely by the proposed AHLD, leaving only sea region. After the removal operation, the ship target segmentation in the sea region can be simply treated as two-class (ship target class and sea background class) gray-level classification problem, where the ship target belong to one set of gray levels and the sea background to the others [3]. Recall that the ***Property 2*** of IR images, the main body of ship target is much smaller than sea background, and they have different gray-level intensity features. In other words, the much larger proportion of sea background pixels is

Algorithm 1 Proposed automatic horizon line detection (AHLD) algorithm.

Input: The original IR ship image f.

Output: Obtain the IR image of only the sea region (including ship target and sea background).

1: Compute the structure tensor (ST) of IR ship image f according to (2)-(6).
2: Calculate the large eigenvalues of structure tensor (STLE) map by using (7).
3: Achieve the binary STLE (BSTLE) map according to (8) and (9).
4: Search the longest straight line on BSTLE map by Hough transform as the potential horizon line according to (10) and (11).
5: Compute the standard metric γ of the potential horizon line by using (12).
6: **If** the standard metric γ is larger than 0.7 **do**
The horizon line exists and the sky/land regions are removed.
Else
The horizon line absents and the whole original IR image f are remained.
End if

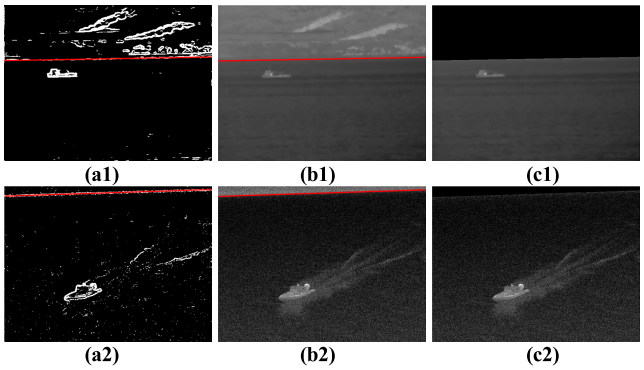

FIGURE 4. The results of the detected horizon line and the sky/land region removal by the proposed AHLD method. (a) The longest straight-line extraction in BSTLE map. (b) The corresponding horizon line detection in the IR ship image. (c) The sky/land region removal by the proposed AHLD method.

present in the IR ship image and dominates the gray-level histogram of image. Thus, the gray-level histogram distribution of IR ship target and sea background would be unimodal or close to unimodal. That is, the secondary peak (corresponding to ship target) is either very small, or submerged within the main peak (corresponding to sea background). Currently, most studies focus on bright IR ship target segmentation, where the background is the comparatively dark sea surface and the ship targets are the relatively brighter regions, and the sketch of unimodal threshold for bright ship target is shown in Fig. 5(a) [22], [25]. However, in real cases, dark ship targets whose infrared radiation is lower than surroundings also exist in the backlighting IR images [15], [26], [34]. Analogous to Fig. 5(a), the sketch of unimodal threshold for dark ship target can be deduced as Fig. 5(b).

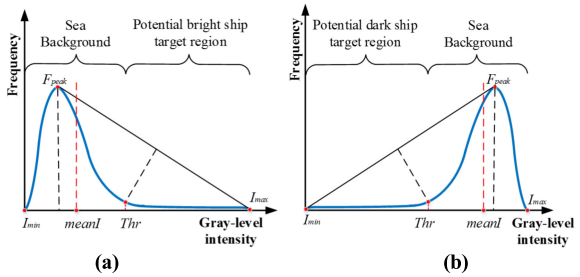

FIGURE 5. The sketches for unimodal threshold of gray-level histogram of IR ship target and sea background. (a) The sketch of unimodal threshold for bright ship target [22], [24]. (b) The sketch of unimodal threshold for dark ship target.

References [35]–[37] indicated that for unimodal histogram of image, the Kapur's maximum histogram entropy (MHE) method [38] can successfully find the reasonable threshold value that locates at the bottom valley of the single peak histogram distribution. Inspired by this vision, in view of the fact that the gray-level histogram distribution of IR ship target and sea background would also be unimodal or close to unimodal as analyzed in the above part, we adopt MHE [38] to accurately perceive the brightness (relative bright or dark) of ship target, and adaptively segment the ship target from sea background. Concisely, let $p(j)$ be the probability of each gray-level j of the region (i.e. sea region) below the horizon of the IR ship image after the sky/land region removal operation. Then, the information entropy of gray-level histogram of two classes (might be ship target class and sea background class) can be written as:

$$\begin{cases} H_d(I) = = -\sum_{j=I_{\min}}^{I} \left[\frac{p(j)}{p(D)} \ln \left(\frac{p(j)}{p(D)} \right) \right], & \text{Dark class} \\ H_b(I) = -\sum_{j=I}^{I_{\max}} \left[\frac{p(j)}{1-p(D)} \ln \left(\frac{p(j)}{1-p(D)} \right) \right], & \text{Bright class} \end{cases} \tag{13}$$

where $H_d(\bullet)$ and $H_b(\bullet)$ are the information entropy of gray-level histogram of dark class and bright class, $p(D) = \sum_{j=I_{\min}}^{I} p(j)$ is the probability distribution of the dark class, and $I \in [I_{\min}, I_{\max}]$ denotes a threshold that should be determined to divide these two classes. According to the maximum entropy principle [38], the optimal threshold Thr to divide them is satisfied to:

$$Thr = \arg \max_{I \in [I_{\min}, I_{\max}]} [H_d(I) + H_b(I)] \tag{14}$$

After the calculation of the MHE, the IR image is divided into bright class and dark class by the computed optimal threshold Thr. In the real-world IR maritime scenes, the global-contrast brightness (bright or dark) of ship target is unknown, so the adaptive ship target segmentation for both bright and dark ones in IR image remains to be worthy of further investigation. As Fig. 5 demonstrates, because the much larger proportion of sea background pixels dominates the histogram, the average intensity value of the IR ship image after the sky/land region removal operation will be located

Algorithm 2 Presented adaptive maximum histogram entropy (AMHE) algorithm.

Input: The IR ship image f after sky/land region removal.
Output: Obtain the coarse segmentation result of IR ship target.

1: Plot the gray-level histogram of the region (i.e. sea region) below the horizon of the IR ship image after the sky/land region removal operation, and count the probability $p(j)$ of each gray-level j of the sea region.
2: Find the optimal threshold Thr to divide the IR ship image into dark class and bright class using (13) and (14).
3: Calculate the average intensity value $meanI$ of the sea region of IR ship image with (15).
4: Compare the computed optimal threshold Thr and average intensity value $meanI$ to accurately perceive the main body brightness (bright or dark) of ship target.
5: Segment the bright or dark IR ship target from sea background according to (16).

near the peak frequency F_{peak} in the gray-level histogram, and the average intensity value $meanI$ is:

$$meanI = \frac{1}{N_{Sea}} \sum_{x=1}^{Width} \sum_{y=kx+b}^{Height} f(x, y) \tag{15}$$

where N_{Sea} denotes the cardinality of the sea region pixel data, and $(x, y) \in \mathbb{R}^{[1:Width, kx+b+1:Height]}$ represents the sea region after the sky/land region removal operation. Note that here y starts with 1 if the horizon line absents. According to the shape property of the unimodal gray-level histogram shown in Fig. 5, we conclude that the computed optimal threshold Thr is usually located at the right-side (left-side) of the average intensity value $meanI$ when the main body of IR ship target is relatively bright (dark) compared with the sea background. Based on this conclusion, the adaptive maximum histogram entropy (AMHE) for automatically segmenting IR ship target from sea background is presented, and can be defined as:

$$AMHE(x, y) = \begin{cases} 1, & if\ (f(x, y) > Thr\ \&\ Thr \geq meanI) \\ & \|\ (f(x, y) < Thr\ \&\ Thr < meanI) \\ 0, & otherwise \end{cases} \tag{16}$$

where $(x, y) \in \mathbb{R}^{[1:Width, kx+b+1:Height]}$. $Thr \geq meanI$ indicates that the sea background (much larger proportion) is the dark class, and the bright class $f(x, y) > Thr$ will be regarded as the ship target. Similarly, if $Thr < meanI$, it indicates that sea background (much larger proportion) is the bright class, and the dark class $f(x, y) < Thr$ will be regarded as the ship target. The whole of the presented adaptive maximum histogram entropy (AMHE) method for adaptively segmenting bright or dark IR ship target from sea background is summarized in **Algorithm 2**.

Fig. 6 shows the IR ship target segmentation results of the presented AMHE. As can be seen from Fig. 6(b), without loss

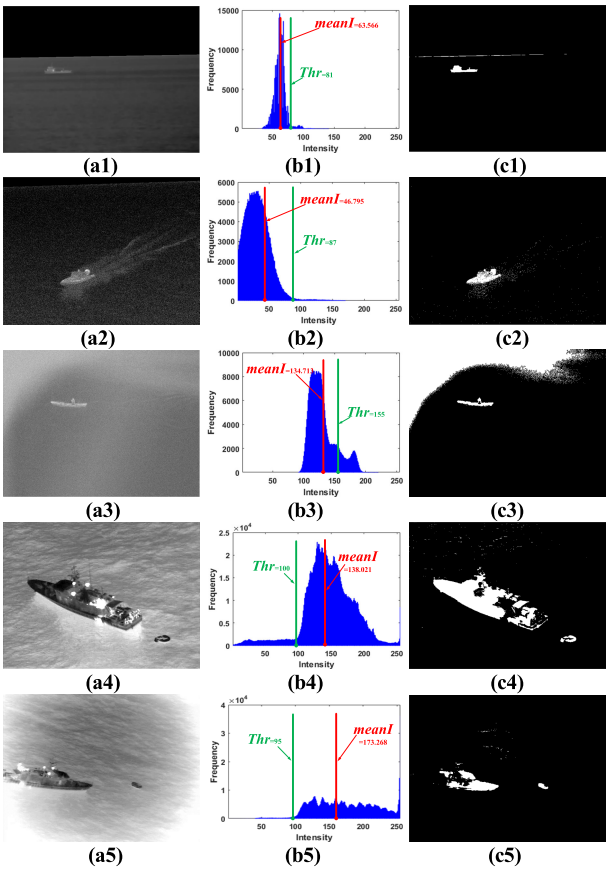

FIGURE 6. Segmentation results of the proposed AMHE. (a) The IR ship images only include ship target and sea background after the AHLD operation. (b) The gray-level histograms of (a), and the mean value (marked by red line) and computed threshold (marked by green line) can adaptively indicate the main body brightness of ship target. (c) The ship target segmentation results of the proposed AMHE.

of generality of the shape of unimodal gray-level histogram, the gray-level histograms of ship target and sea background obey the analyzed unimodal distribution model. Thereby, the presented AMHE method can accurately perceive the brightness (bright or dark) of ship target, and automatically segment the ship target from the sea background, as Fig. 6(c) illustrates. However, the segmentation results of AMHE are relatively coarse. Although most of clutters with uneven intensity can be eliminated after the sky/land region removal operation, the sea region may also have some intensity inhomogeneity parts whose gray-level intensity is close to the ship target. Accordingly, as shown in Fig. 6(c1) and (c3), the AMHE can separate the IR ship targets from sea background, but it introduces some background clutters into the results, and generates under-segmentation phenomena. Furthermore, the AMHE is also affected by noise and fluctuating sea clutters, as Fig. 6(c2), (c4) and (c5) shows. More seriously, for large IR ship targets with uneven intensities, although the AMHE can detect the brightness and segment the main body of ship target, the parts of the ship target with opposite or indistinctive intensities will be mistakenly divided into background and missed, as shown in Fig. 6(c4) and especially Fig. 6(c5). These are because the AMHE only takes the

gray-level intensity distribution property of IR ship target and sea background into the consideration, which may lead to under-segmentation or over-segmentation phenomena in different degrees. To overcome these problems, the boundary information of ship target is reasonably incorporated into the next refinement step of IR ship target segmentation.

VI. TWO-STEP REFINEMENT FOR IR SHIP TARGET SEGMENTATION

A. MHE GUIDED GRAY-LEVEL MORPHOLOGICAL RECONSTRUCTION

The IR ship images are usually affected by heavy sea clutters, high noise levels and uneven intensities, which increases the difficulty of real boundary extraction of ship target, as shown in Fig. 2. Therefore, an effective filter processing is necessary to mitigate those disturbances and improve the boundary characteristics of ship target. In our previous work [26], we have suggested that the closing-based (opening-based) gray-level morphological reconstruction (GMR) operation [39], [40] can be efficiently used for pre-processing bright (dark) IR ship image to suppress heavy sea clutters and noise components and enhance the contour feature of ship target. However, if the brightness (bright or dark) of the ship target relative to the background is unknown in advance, the classical GMR-based pre-processing procedure cannot be adaptively selected to filter the IR ship image. Fortunately, as analyzed in above *Section V*, the main body brightness of ship target can be accurately perceived according to the comparison of the optimal threshold *Thr* computed by MHE and average intensity value *meanI*. Therefore, combining their advantages to adaptively smooth bright or dark IR ship image, the MHE guided gray-level morphological reconstruction (EGMR) filter is designed as follows:

$$EGMR(x,y) = \begin{cases} CGMR[f(x,y)], & if\ Thr \geq meanI \\ OGMR[f(x,y)], & else\ Thr < meanI \end{cases} \quad (17)$$

where $(x,y) \in \mathbb{R}^{[1:Width, kx+b+1:Height]}$. $CGMR(\bullet)$ and $OGMR(\bullet)$ denote the closing- and opening-based GMR operators, respectively. Here $Thr \geq meanI$ ($Thr < meanI$) indicates that the main body of ship target is bright (dark) relative to the sea background, then the EGMR filter can adaptively select CGMR (OGMR) to smooth the sea region of IR ship image. We compute the STLE map and BSTLE edge map in the sea region after EGMR filtering to obtain the boundary information of ship target, and the recomputed STLE and BSTLE are respectively named as rSTLE and rBSTLE.

Fig. 7 shows the ship target boundary information corrected by the EGMR filter. Comparing Fig. 7(b) with (a), the EGMR can adaptively smooth bright or dark IR ship images, filter heavy noise components as shown in Fig. 7(b2) and (b3) and suppress intricate sea clutters as shown in Fig. 7(b4) and (b5) while preserving the main body brightness and intensity of ship targets. The heavier the noise level and sea clutter are, the more obvious the filtering efficiency of EGMR is. More importantly, the EGMR filter can remove the inner parts of the ship target with strong opposite intensities

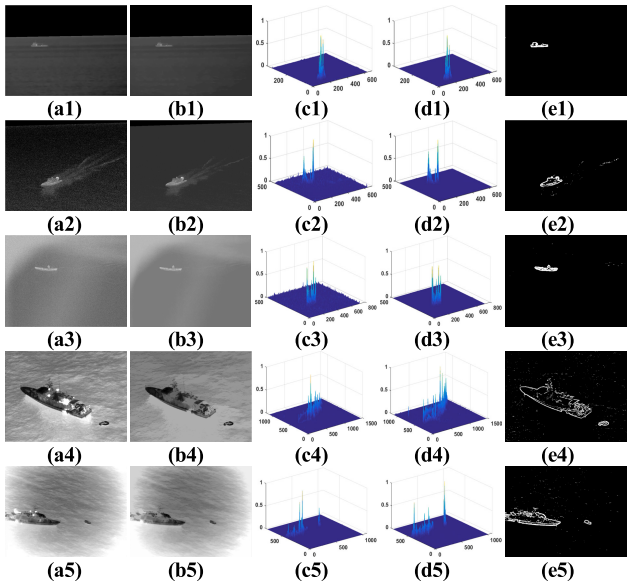

FIGURE 7. The ship target boundary information corrected by the EGMR filter. (a) The original IR ship images. (b) The EGMR filtered IR ship images. (c) The 3-D mesh plots for the STLE map. (d) The 3-D mesh plots for the rSTLE map. (e) The edge maps computed by the designed rBSTLE.

and drive the brightness and intensity of these parts to be more consistent with the gray scale of the main body, as shown in Fig. 7(b4) and (b5). As can be seen from Fig. 2(c) and Fig. 7(c), the STLE map of original IR ship image can generally depict the hull boundaries. However, there are still noise clutters that cannot be ignored, and the local abrupt boundary caused by the ship interior with strong opposite intensity suddenly becomes very large thus inhibiting the real boundary of ship target, which eventually leads to the failure of the idea of using the boundary information to improve the IR ship target segmentation. Because the EGMR can suppress strong noise clutters and make the interior of ship targets with extremely opposite intensity tend to be consistent, the rSTLE map of the EGMR filtered IR images is more robust to heavy noise clutters and can enhance the real hull boundaries of extremely uneven ship target, as Fig. 7(d) illustrates. Finally, by comparing Fig. 7(e) with Fig. 2(c), the rBSTLE edge map of the EGMR filtered IR ship images can completely delineate the boundaries of ship target with much less false edges and noise. Therefore, the rSTLE map and rBSTLE edge map corrected by the EGMR filter can greatly highlight the real boundary information of ship target and effectively suppress false alarms and noise, so as to make it more reliable to refine the IR ship target segmentation by exploiting the boundary information.

B. SHIP FOREGROUND MAP (SFM)

Inspired by the ***Property 3*** of IR ship images, the boundary of ship target is more conspicuous than its surroundings and sea background, and the boundary information of IR ship target can be explicitly delineated by the rSTLE map and rBSTLE edge map on the EGMR filtered IR image.

Based on these positive factors, the boundary information is reasonably incorporated into the refinement step of the IR ship target segmentation. It is noteworthy that the image patch-based processing approach has been proved its success for local image information measure [41]–[44]. In this paper, we also adopt the patch-based approach to locate the regions-of-interest (ROI) of ship target in the rBSTLE edge map for refining the ship target segmentation and reducing computing costs. Firstly, a group of image patches with an image-adaptive window size $S \times S$ is generated by sliding the window from left and top to right and down in the rBSTLE edge map after sky/land region removal operation, and the step length is $S/2$. The image-adaptive window size is chosen as $S = 0.05 \times Width$ of the IR image. Thus, the group of image patches is expressed as:

$$\mathbf{P} = [\mathbf{p}_1, \mathbf{p}_2, \ldots, \mathbf{p}_i, \ldots, \mathbf{p}_{TN}] \in \mathbb{R}^{[1:Width, kx+b+1:Height]} \quad (18)$$

where $\mathbf{p}_i$ is the matrix of the i-th image patch, TN is the total number of image patches. Looking back at Fig. 7(e), the edge pixel number of ship target is much larger than that of sea background in the rBSTLE map. To suppress the residual trivial clutters and check the real boundary patches of ship target in the group of image patches, the rBSTLE-based edge image patches selection method is proposed:

$$\mathbf{p}_i(x', y') = \begin{cases} 1, & E_i \geq \xi \\ 0, & otherwise \end{cases} \quad (19)$$

where E_i denotes the edge strength (i.e. total number of edge pixel in the i-th image patch), (x', y') represents the pixel location in the local patch. The ξ is the empirically threshold of the edge strength, and to select more boundary patches of ship target we use a relatively small value $\xi = 0.05 \times S^2$ in this paper. By the definition of the image patches selection method, if the edge strength E_i of the patch $\mathbf{p}_i$ is larger than the threshold ξ, the patch can be regarded as the boundary patch of ship target and all matrix elements of $\mathbf{p}_i$ are replaced by 1, otherwise by 0.

Then, the selected patches are all-ones matrixes for clustering a new selected group $\mathbf{P}_{Sel} \subseteq \mathbf{P}$, and they are orderly projected into a 2-D array of all-zeros (its size is the same as the original IR ship image) to obtain the regions-of-interest (ROI) map of ship target, which is derived by:

$$ROI_{st}(x, y) = \begin{cases} 1, & \forall (x, y) \in \mathbf{P}_{Sel} \\ 0, & otherwise \end{cases} \quad (20)$$

That means if the location (x, y) belongs to any patch of the new selected group $\mathbf{P}_{Sel}$, the pixel value is set to 1. To further eliminate the interference of sea clutter regions whose gray-level intensity is approximate to the ship target and address the under-segmentation problem of the presented ACHME method, the ship foreground map (SFM) is computed by performing pixel-based logical-AND operator on the AMHE map and the ROI map of ship target:

$$SFM(x, y) = AMHE(x, y) \text{ AND } ROI_{st}(x, y) \quad (21)$$

Algorithm 3 Developed ship foreground map (SFM) algorithm.

Input: The segmentation result map of the AMHE, the IR ship image f after sky/land region removal.

Output: Acquire the ship foreground map (SFM).

1: Smooth the sea region of IR ship image f by the designed EGMR filter according to (17).
2: Calculate the rSTLE map and rBSTLE map in the sea region after EGMR filtering with (2-9).
3: Group a set of patches in the rBSTLE edge map by sliding window step-by-step:
$\mathbf{P} = [\mathbf{p}_1, \mathbf{p}_2, \ldots, \mathbf{p}_i, \ldots, \mathbf{p}_N] \in \mathbb{R}^{[x=1:Width, y=kx+b:Height]}$
4: **For** patch index $i = 1{:}TN$ **do**
If the edge strength E_i of the patch $\mathbf{p}_i$ is larger than the threshold ξ, the patch will be selected as the boundary patch of ship target according to (19);
Cluster the selected patch $\mathbf{p}_i$ as the new selected group $\mathbf{P}_{Sel} \subseteq \mathbf{P}$;
End for.
5: Project the selected patches into the 2-D array of all-zeros to obtain the regions-of-interest (ROI) map of ship target according to (20).
6: Perform logical-AND operator on the AMHE map and the ROI map of ship targets with (21).

The whole of the developed ship foreground map (SFM) method for efficiently locating ship target region and solving the under-segmentation problem is summarized in **Algorithm 3**.

Fig. 8 gives the computation process of the developed SFM. It can be seen from Fig. 8(a) and (b) that the IR ship targets can be accurately masked by the selected image patches according to the rBSTLE-based edge image patches selection method. Hence, the ROI of ship targets can be reliably located via projecting the group of selected patches on a 2-D array of all-zeros with the same size as the original image, as Fig. 8(c) illustrates. Finally, as presented in Fig. 8(d), the developed SFM can efficiently remove the interference of sea clutter regions whose gray-level intensity is approximate to the ship target and solve the under-segmentation problem, especially for Fig. 8(d1) and (d3). This is because the SFM properly integrates gray-level intensity information and boundary information constraint to extract the ship targets from the sea background and can largely eliminate the redundant complex background clutters. However, although the SFM can accurately segment the main body of ship targets from sea background, it still cannot alleviate the phenomena of over-segmentation, as Fig. 8(d2), (d4) and (d5) demonstrates. To cope with over-segmentation of IR ship target, a modified Watershed transform is further constructed in the next part by fully taking the advantages of maximum histogram entropy and large eigenvalues of structure tensor.

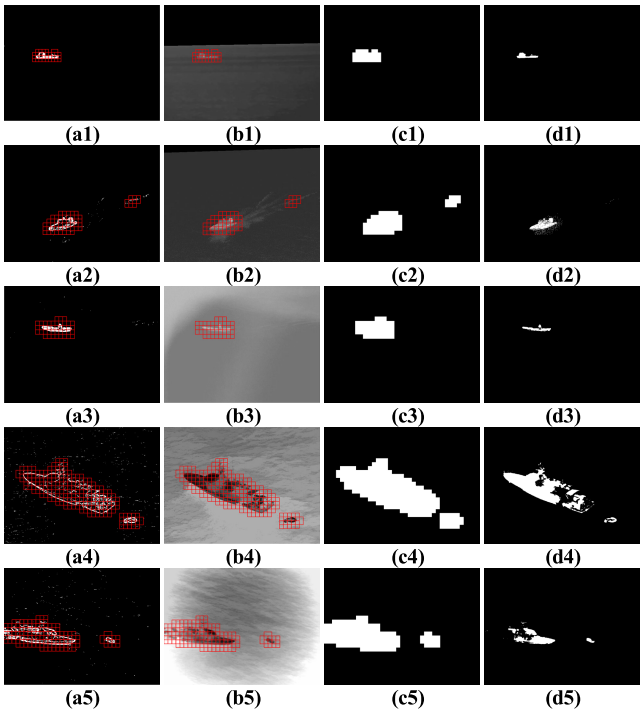

FIGURE 8. The computation process of ship foreground map (SFM). (a) The red boxes in the rBSTLE edge maps have outlined the finally selected image patches. (b) The red boxes on the EGMR filtered IR ship images have marked the selected patches. (c) The obtained ROI map of ship target. (d) The results of the developed SFM.

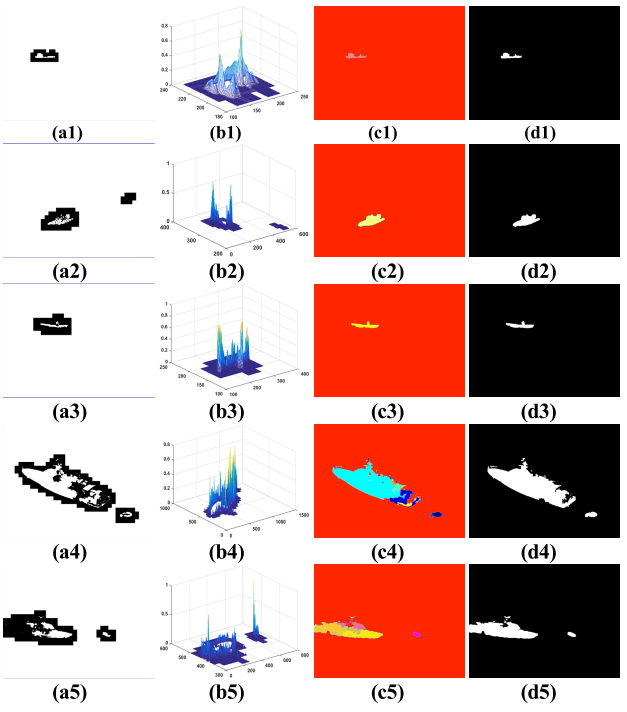

FIGURE 9. The final IR ship segmentation results. (a) The extracted marker images. (b) The obtained FRBI of ship targets as the watershed lines. (c) The watershed regions are labeled by different colors. (d) The final ship target segmentation results after the ETWT processing.

C. STRUCTURE TENSOR AND MAXIMUM HISTOGRAM ENTROPY MODIFIED WATERSHED TRANSFORM (TEWT)

The marker-controlled gradient based Watershed transform (MGWT) strategy can incorporate the advantages of both region-based (pixel similarity) and edge-based (pixel discontinuity) techniques to helpfully reduce the over-segmentation problem and is practical for the quick and effective post-processing of large size image [45]–[47]. The marker extraction and boundary representation are two key issues for MGWT methods, which directly determine the effects of its segmentation. If the extraction of marks is unreasonable or the indistinctive boundary cannot be depicted well, the segmentation effect of MGWT will decrease sharply. With the consideration that the object boundaries cannot pass through the marker image in the MGWT method, the boundary information is rectified according to the marker image to get the final boundary information of ship target that is more appropriate to the reality. Depending on this point, we use the SFM eroded with three-pixel disk-shaped structuring element SFM_{ero} as the internal marker coincided with objects of interest, and utilize the complement of the ROI map of ship target $\overline{ROI_{st}}$ as the external marker associated with background. The marker image can be easily extracted by performing logical-OR operator on the internal marker and the external marker:

$$I_{Marker}(x, y) = SFM_{ero}(x, y) \text{ OR } \overline{ROI_{st}}(x, y) \tag{22}$$

By the definition of the extracted marker image I_{Marker}, the background (i.e. the external marker part) will be clipped out and the main body of ship target (i.e. the internal marker part) will be labeled as seed regions for the catchment basins of Watershed transform, as Fig. 9(a) shows. Recall that the rSTLE map is robust to heavy noise clutters and can completely depict the real hull boundaries of extremely uneven ship target without introducing spurious edges. Therefore, the rSTLE map can be further imposed to the minima by the extracted marker image to obtain the final rectified boundary information (FRBI) of ship target:

$$FRBI(x, y) = \begin{cases} rSTLE(x, y), & I_{marker}(x, y) = 0 \\ -Inf, & otherwise \end{cases} \tag{23}$$

where $-Inf$ denotes the negative infinity $-\infty$ for punching the holes in each regional minimum. Hence, the FRBI of ship target can be constructed as the watershed ridgelines for Watershed transform, as Fig 9(b) illustrates. The FRBI fully integrates the both advantages of maximum histogram entropy and large eigenvalues of structure tensor, and can be efficiently exploited to modify the Vincent's Watershed transform [48] for totally segmenting ship target. Suppose that the FRBI of ship target as the watershed line is the dam, and that the catchment basins are entirely flooded by letting water rise through the punched holes until the last state is reached when only the top of the dam is visible above the waterline. The last state corresponds to the desired segmentation result of Watershed transform, and the pixels are labeled

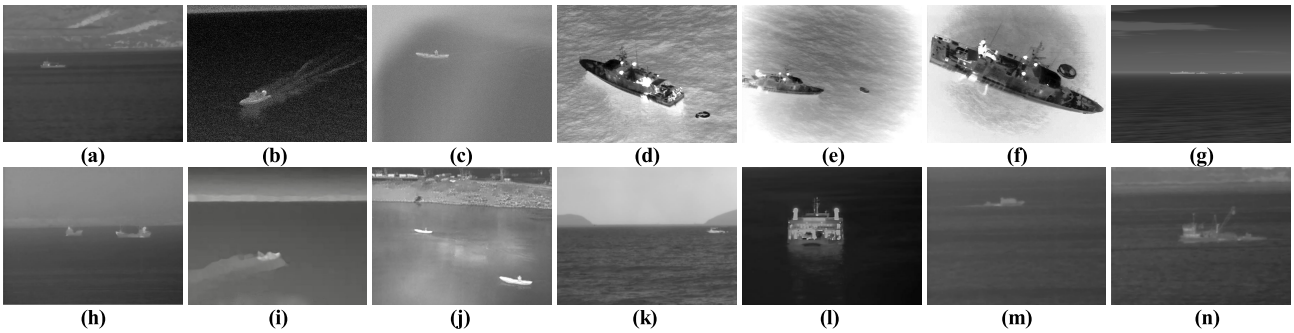

FIGURE 10. Representative IR ship images of the test dataset.

Algorithm 4 The structure tensor and maximum histogram entropy modified Watershed transform (TEWT).

Input: The SFM, the ROI map of ship target, and the rSTLE map.

Output: Obtain the final IR ship target segmentation result.

1: Extract the marker image I_{Marker} by performing logical-OR operator on the eroded SFM and the complement of the ROI map with (22).
2: Impose the rSTLE map into the minima by the extracted marker image I_{Marker} to obtain the final rectified boundary information $FRBI$ of ship target, according to (23).
3: Construct the structure tensor and maximum histogram entropy modified Watershed transform $TEWT$ derived from (24) to extract the whole IR ship target.

into different watershed regions, as Fig 9(c) demonstrates. Finally, a new Watershed algorithm named as the structure tensor and maximum histogram entropy modified Watershed transform (TEWT) for IR ship target segmentation is constructed, and can be simply written as:

$$TEWT(x,y)=\begin{cases}1, & Labeling\left[Watershed\left(FRBI(x,y)\right)\right]>1\\ 0, & Labeling\left[Watershed\left(FRBI(x,y)\right)\right]=1\end{cases} \tag{24}$$

where $Watershed(\bullet)$ represents the Vincent's Watershed transform [48], $Labeling(\bullet)$ denotes the labeling method sorted according to the pixel number of each region. The pixels labeled 1 belong to the biggest watershed region, the pixels labeled 2 belong to the second biggest watershed region, and so on. It can be seen from Fig 9(c), since the FRBI of ship target as an effective barrier for the water flow, the biggest watershed region corresponding to the background marked by orange color can be entirely isolated, and the other watershed regions marked by randomly shuffled colors would belong to ship target. Therefore, we assign the pixels labeled 1 as the background, and merge the pixels labeled greater than 1 as the ship target. The whole of the constructed structure tensor and maximum histogram entropy modified Watershed transform (TEWT) for efficiently addressing the over-segmentation problem is summarized in **Algorithm 4**.

Fig. 9 shows the final IR ship segmentation results after the ETWT processing. As shown in Fig. 9(a), the marker images is accurately extracted by performing logical-OR operator on the eroded SFM and the complement of the ROI map. The rSTLE map is further imposed to the minima by the extracted marker image to obtain the FRBI of ship targets, as Fig. 9(b) shows. Since the FRBI of ship targets as an effective barrier for the water flow, the biggest watershed region corresponding to the background marked by orange color can be entirely isolated and the other watershed regions would belong to ship target, as Fig. 9(c) shows. Finally, by fully integrating the both advantages of maximum histogram entropy and large eigenvalues of structure tensor, the IR ship targets can be almost completely segmented after the constructed TEWT post-processing, and there is scarcely residual clutter in the final segmentation results, as illustrated in Fig. 9(d).

VII. EXPERIMENTAL RESULTS AND ANALYSIS

In this section, a series of experiments on IR ship images under various maritime scenes are conducted to validate the accuracy and effectiveness of the proposed automatic IR ship target segmentation algorithm. Furthermore, some classical algorithms and state-of-the-art algorithms are selected for performance comparison. These experiments are performed in Matlab 2016a on the computer with 3.2 Ghz Intel i5-6500 CPU and 16 Gb random access memory.

A. TEST DATASET

The test dataset is composed of 200 IR ship images, which are collected from diverse sources, including the maritime detection, classification and tracking (MarDCT) dataset [49], the PETS2016 dataset [50], the Al Salam Boccaccio 98 images (ASB98i) [51], and our own captured dataset (OCD). Fig. 10 shows 14 representative IR ship images of the test dataset used for visual performance evaluation, and each image represents a typical maritime scenario in IR ship detection applications. These IR ship images are labeled as Img.1∼14. Fig. 10(a) describes an obscure ship target disturbed by intricate land clutters but with weak coastline. Fig. 10(b) is a bright ship target corrupted by strong long-tail waves and heavy Gaussian noise in sea-sky background.

TABLE 1. Detail information of the test IR ship images.

Images	Image sizes	Target brightness	Target areas	Target number	Horizon exists	Datasets
Img.1	640×480	Bright	905	1	Yes	MarDCT
Img.2	640×480	Bright	3186	1	Yes	PETS2016
Img.3	720×480	Bright	1722	1	No	OCD
Img.4	1450×1107	Dark	145965	1	No	ASB98i
Img.5	1024×775	Dark	30537	1	No	ASB98i
Img.6	1024×778	Dark	177654	1	No	ASB98i
Img.7	1280×1024	Bright	167-3465	4	Yes	OCD
Img.8	611×512	Bright	938-3692	2	Yes	MarDCT
Img.9	640×480	Bright	1215	1	Yes	PETS2016
Img.10	720×480	Bright	536-1796	2	Yes	OCD
Img.11	640×480	Bright	474	1	Yes	OCD
Img.12	611×512	Bright	13639	1	No	MarDCT
Img.13	640×480	Bright	2175	1	No	MarDCT
Img.14	611×512	Bright	9521	1	Yes	MarDCT

Fig. 10(c) is the bright ship target interfered by the bright sea clutter regions whose gray-level intensity is close to the ship target and Gaussian noise. Fig. 10(d) is a huge and dark ship target with uneven intensities submerged in heavy sea clutters. Fig. 10(e) and (f) describe a large and dark ship target with extremely uneven intensities, half of which is buried in inhomogeneous sea background. Fig. 10(g) depicts four synthesized ship targets with different sizes appearing near the sea-sky-line. Fig. 10(h) displays two bright ship targets located in a relatively mild sea and sky background. Fig. 10(i) is a low-contrast and fast-moving ship target surrounded by tail wave interference. Fig. 10(j) shows two bright ship targets interfered by bright sea clutter regions, cars and land clutters. Fig. 10(k) is a bright ship target under a heterogeneous background with sea, sky and islands. Fig. 10(l) shows a bright uneven ship target appeared in a mild sea background. Fig. 10(m) and (n) describe an extremely ambiguous ship target almost completely embedded in the sea background. Table 1 lists the detail information about the test IR ship images. Accordingly, the test images are variable in scene type, clutter type, target type, target size, target quantity, and image size. Testing on this dataset proves that the algorithm is suitable for different ship targets in many IR maritime scenarios.

B. RESULTS OF INFRARED SHIP SEGMENTATION

1) PARAMETER SETTINGS

As above *Section IV* analysis, the standard metric γ fully considers the length, slope and edge thickness of the detected line to determine whether it is the horizon line, and γ of IR ship images with horizon line is almost much larger than that of IR ship images without horizon line. Accordingly, in the experiment, we randomly selected 45 IR ship images with horizon line and 45 ship images without horizon line, and computed their standard metric γ one by one. The computed γ of the selected IR ship images are shown in Fig. 11.

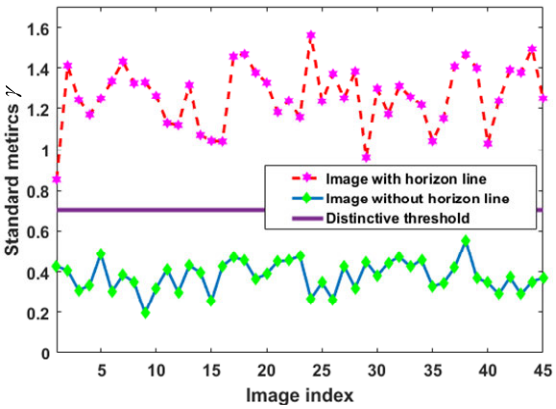

FIGURE 11. The standard metrics γ of IR ship images and the experimentally selected distinctive threshold $\gamma*$.

The red point line denotes the γ of the images with horizon line, and the green point line denotes the γ of the images without horizon line. As can be seen from Fig. 11, because the standard metrics γ of IR images with or without horizon line have a distinctive discrimination, the OTSU method [52] is utilized to find the optimal distinctive threshold:

$$\gamma* = OTSU(\gamma) \tag{25}$$

where $\gamma = [\gamma_1, \gamma_2, \ldots, \gamma_j, \ldots, \gamma_{90}]$ is the group of standard metrics of IR ship images, and j denotes the image index. Then, the computed distinctive threshold $\gamma* = 0.7020$ can be used to clearly discriminate the existences of horizon line in IR ship images, as drawn by the purple line in Fig. 11. Therefore, the distinctive threshold is empirically set $\gamma* = 0.7$ in our experiments to reliably judge whether the horizon line exists.

Table 2 lists the standard metric γ of the potential horizon line of each test IR image. The standard metrics γ of Imgs.1, 2, 7-11, and 14 are much larger than the distinctive

TABLE 2. Standard metrics of the potential horizon line in test IR images.

Images	Img.1	Img.2	Img.3	Img.4	Img.5	Img.6	Img.7
γ	1.2718	1.3395	0.3437	0.4098	0.4419	0.4672	1.2498
	Img.8	Img.9	Img.10	Img.11	Img.12	Img.13	Img.14
	1.1153	1.4289	1.1343	1.3937	0.3142	0.4528	1.0629

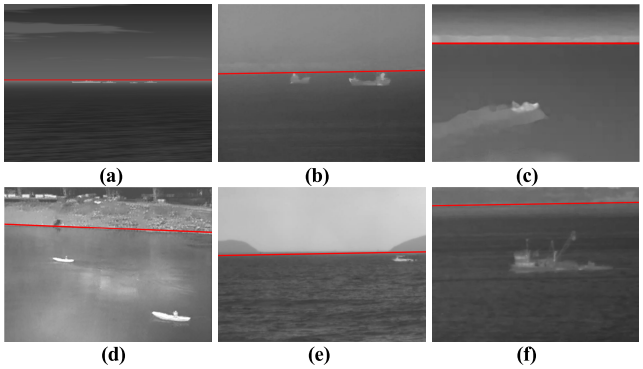

FIGURE 12. Results of the final detected horizon line by the proposed AHLD method.

threshold $\gamma* = 0.7$, and their corresponding results of detected horizon line by the proposed AHLD method are shown in Fig. 4 and Fig. 12, meanwhile the γ of Imgs.3-6, 12, and 13 are much smaller than the distinctive threshold. Accordingly, the existence of horizon line in each IR ship image can be accurately judged by the suggested standard metric and distinctive threshold, and the sky or land region clutters can be reliably removed by the proposed AHLD method.

2) VISUAL COMPARISON TO IR SHIP TARGET SEGMENTATION BASELINE METHODS

In this part, three classical ship target segmentation methods and five state-of-the-art ship target segmentation methods are introduced in the comparison experiments to evaluate the performance of the proposed IR ship target segmentation method. The weighted entropy induced Markov random field (WEMRF) [7], the 2-D maximum entropy (2DME) [11], [12], and the mean shift segmentation (MSS) [21] are chosen as the representative classical ship target segmentation methods. The fuzzy correlation based graph cut scheme (FCGCS) [16], the entropy energy driven Chan–Vese model (ECVM) [20], the multi-feature integration (MFI) [22], the Markov random filed constraint spatial fuzzy c-means method (MRF-SFCM) [1], [24], and the morphological reconstruction based multi-feature analysis (MRMFA) [26] are selected as the representative state-of-the-art methods. Because those methods have been well studied, they can be used for assessing the performance of the new IR ship target segmentation method. The detailed parameter settings of the compared algorithms are summarized in Table 3.

Fig. 13 shows the IR ship target segmentation results of different methods for Fig. 10. The original IR ship images with different ship targets in different backgrounds are shown in Fig. 13(a), the initial curves (manually set) of the ECVM method are indicated in Fig. 13(b), and the ground-truth segmentation images (manually labeled) are listed in Fig. 13(l). The WEMRF method firstly calculates the initial segmentation by utilizing variance weighted information entropy (WIE) to locate the ROI, and then separates the ship targets from the background by using the Gaussian MRF with the iterated condition mode (ICM). The WIE can roughly locate the ship target region and boundary, and the MRF is commonly used for background modeling via capturing the spatial constraints among pixels, hence the method can extract the ship targets with high local contrast, as presented in Fig. 13(c1), (c3), (c11) and (c12). However, due to the characteristics of low SNR, low SCR and complex background of the IR ship images, the MRF-based model is easily classify some of the background into the foreground, so the WEMRF will produce under-segmentation phenomena, as shown in Fig. 13(c1)–(c14). The 2DME is a threshold processing method based on 2-D histogram analysis of the image. When the pixel intensity percentage between the ship target and the background is relatively obvious, the method can find the optimal threshold by the 2D maximum entropy for segmenting the ship targets, as shown in Fig. 13(d4), (d6) and (d12). However, the method only considers the gray-level intensity distribution and is sensitive to the pixel percentage of ship target and background. Therefore, it can be seen from Fig. 13(d1)–(d3), (d5), (d7)–(d11) and (d13) that the method will generate under- or over-segmentation results for the complex and heterogeneous backgrounds. The MSS is a feature-space analysis algorithm based on graph region merging, so it can efficiently extract the regions of ship targets against a homogenous background, as shown in Fig. 13(e3) and (e12). Nevertheless, the MSS does not work well for the environmental maritime conditions with multiple background types, as Fig. 13(e1), (e2) and (e7)–(e11) shows. More seriously, the MSS method cannot segment the ship targets with low contrast or too large, because they will be merged into the background during the region merging process, as Fig. 13(e4)–(e6), (e9), (e13) and (e14) illustrates.

The FCGCS method uses the maximum 2-parition fuzzy correlation model to compress the dark pixels interval and enhance the bright pixel region for achieving segmentation threshold, and implements the graph cut to optimize the segmentation result, so this method can segment the relatively bright ship target even with low contrast, as displayed in Fig. 13(f9) and (f12)–(f14). Unfortunately, since the FCGCS only takes the intensity information of IR ship image into consideration, the background clutter which has the similar gray level as the ship target still cannot be suppressed, as Fig. 13(f1)–(f8), (f10) and (f11) displays. It should be noted that because the 2DME, MSS, and FCGCS methods cannot perceive the brightness of ship target, they all fail to extract the dark ship target from the brighter maritime background for Fig. 13(a4)–(a6). The ECVM extracts ship targets through seeking the closed contours by the

TABLE 3. Parameter settings of the compared methods.

Methods	Acronyms	Categories	Parameter settings
Weighted entropy induced Markov random field	WEMRF	Background modeling-based.	ROIs' parameters: k=1.5, α=6; Maximum iterations: 15.
2-D maximum entropy	2DME	Thresholding-based.	Maximum iterations: 30.
Mean shift segmentation	MSS	Feature analysis-based.	Filter bandwidth: h_s=6.5, h_r=7; Spanning tree threshold: 3.
Fuzzy correlation based graph cut scheme	FCGCS	Thresholding-based.	Fuzzy assessment: ε=0.28; Tuning factor: α=13.
Entropy energy driven Chan–Vese model	ECVM	Active contour-based.	Weighting parameters: λ_1=λ_2=1, μ=0.5; Maximum iterations:500.
Multi-feature integration	MFI	Feature analysis-based.	Iteration number: N_m=6; Shape ranges: t_c=0.1-0.6, R_{wh}=1-9.
Markov random filed constraint spatial fuzzy c-means method	MRF-SFCM	Feature analysis-based; Background modeling-based.	Cluster center number: c=3; Fuzzifier value: q=2.
Morphological reconstruction based multi-feature analysis	MRMFA	Feature analysis-based.	Shape ranges: R_{mm}=1.1-8.8, C_p=11.3-118.6.

local entropy energy driven curve evolution and iterative convex optimization, and it can successfully segment ship targets with topology structure information, as presented in Fig. 13(g1), (g3) and (g12)–(g14). Whereas, because sea clutter will destroy the topology structure of ship targets and the islands may also have strong contour information, the segmentation results of ECVM method will be greatly affected, as Fig. 13(g2) and (g4)–(g11) demonstrates. In addition, the method must manually set the initial contour placement, as indicated in Fig. 13(b), and is vulnerable to the maximum iterations, as listed in Table 3. The MFI method reasonably uses two approaches including iterative global thresholding and ship shape constraints to segment ship targets, hence the MFI presents better performance than the above four classical methods for ship targets with even intensity, as shown in Fig. 13(h2), (h3), (h7)–(h11) and (h13). The MFI is based on the assumption that the ship target region is even and much brighter than the background, so it cannot successfully segment the whole ship targets with uneven intensity, as Fig. 13(h12) and (h14) shows, and almost completely discards the real dark ship targets buried in a brighter sea background, as Fig. 13(h4)–(h6) shows. In the MRF-SFCM method, the Gaussian filter and top-hat transform are firstly used to smooth background, and then the MRF constrained fuzzy c-means clustering is applied for ship target segmentation. It uses nonlocal spatial information and spatial contour shape information to improve the performance of FCM and gets satisfactory results in most cases, as depicted in Fig. 13(i1), (i3), (i7), (i8), and (i10)–(i13). However, due to the interferences of noise, sea clutter and tail waves, the contour of the ship target is ambiguous, resulting in insufficient or excessive segmentation, as presented in Fig. 13(i2), (i9) and (i14). Moreover, as the top-hat transform will overwhelm the dark ship target, those pixels belonging to the ship target will be regarded as background and will not be extracted, as shown in Fig. 13(i4)–(i6). The MRMFA integrates multiple features after GMR operation, including intensity, local contrast, contour, and shape features, and the effect is excellent for both bright and dark ship targets with uniform intensity and obvious local contrast, as depicted in Fig. 13(j1), (j3), (j7), and (j9)–(j11). However, because the method also regards the ship targets as uniform regions under the sea background in IR images due to long imaging distance, the method obtains poor performance for segmenting the whole ship target with uneven intensities in near-distance IR imaging, as presented in Fig. 13(j2), (j4)–(j6), (j8), and (j12)–(j14).

Nevertheless, from Fig. 13(k1)–(k14), it can be seen that the proposed method can precisely segment all the ship targets with lowest false alarms and is more robust than other compared eight methods, especially for the ship targets with unknown brightness, and uneven intensity. This robustness is attributed to the reasonable integration of good performances of structure tensor and maximum histogram entropy according to the intrinsic IR imaging characteristics between ship target and background clutter. Firstly, based on the scene context clue, the AHLD is proposed to efficiently judge the existence of horizon line and remove sky/land region clutters. Then, in view of the intensity distribution of the ship target and the sea background would be unimodal, the AMHE is presented to accurately perceive the brightness (dark or bright) of ship target, and coarsely segment the bright or dark ship target from sea background. Finally, considering the ship target boundary information, the SFM is developed to eliminate residual clutter regions whose gray-level intensity is approximate to the ship target and address the under-segmentation. Additionally, via fully integrating the both advantages of maximum histogram entropy and large eigenvalues of structure tensor, a new modified Watershed algorithm namely TEWT is constructed to completely extract

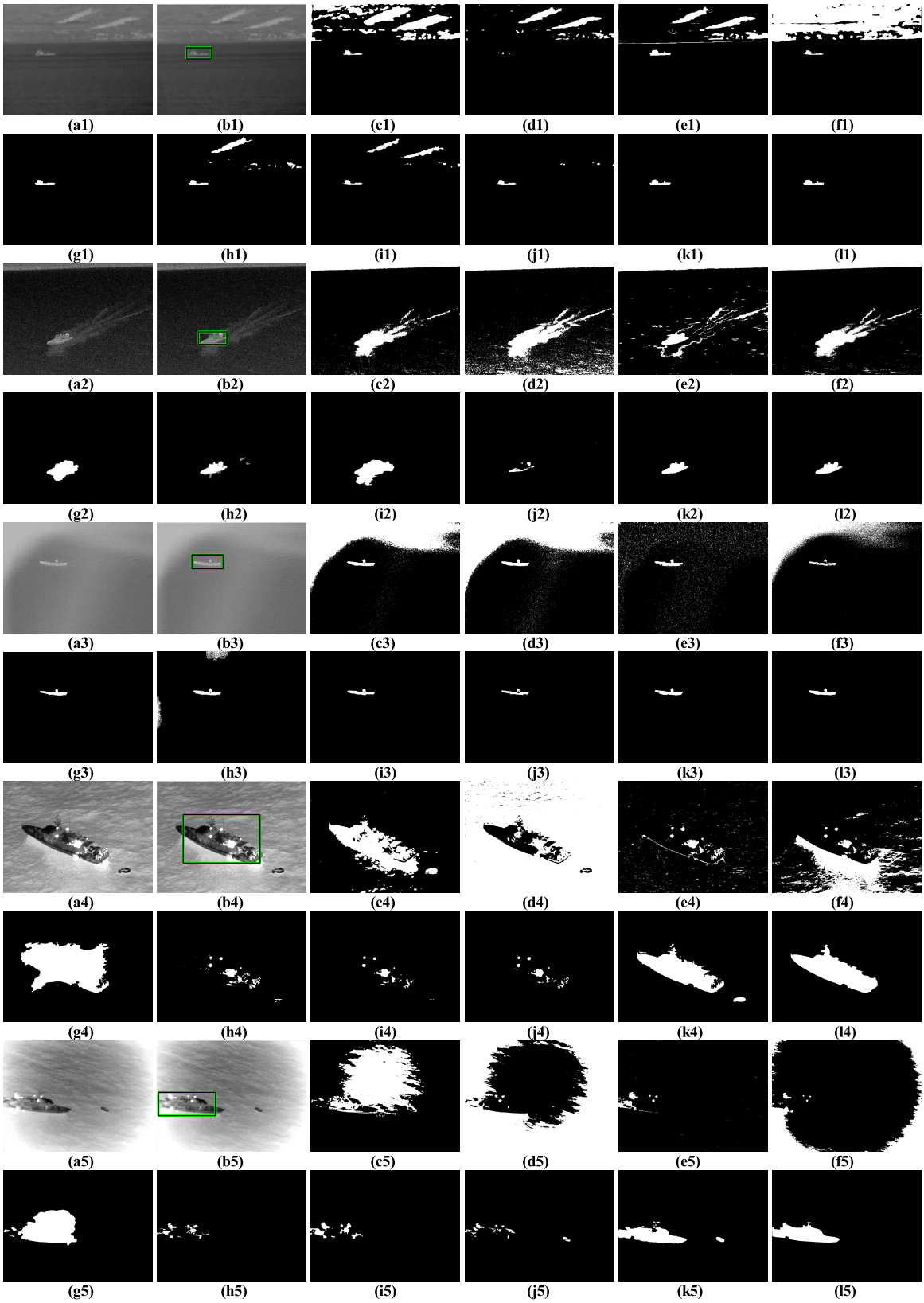

FIGURE 13. Segmentation results of different methods for the Figure 11. (a) The original IR ship images; (b) The initial curve (manually set) of the ECVM; (c)The segmentation results of WEMRF; (d) The segmentation results of 2DME; (e) The segmentation results of MSS; (f) The segmentation results of FCGCS; (g1-9) The segmentation results of ECVM; (h) The segmentation results of MFI; (i) The segmentation results of MRF-SFCM; (j) The segmentation results of MRMFA; (k) The segmentation results of the proposed method; (l) The ground-truth segmentation images (manually labeled).

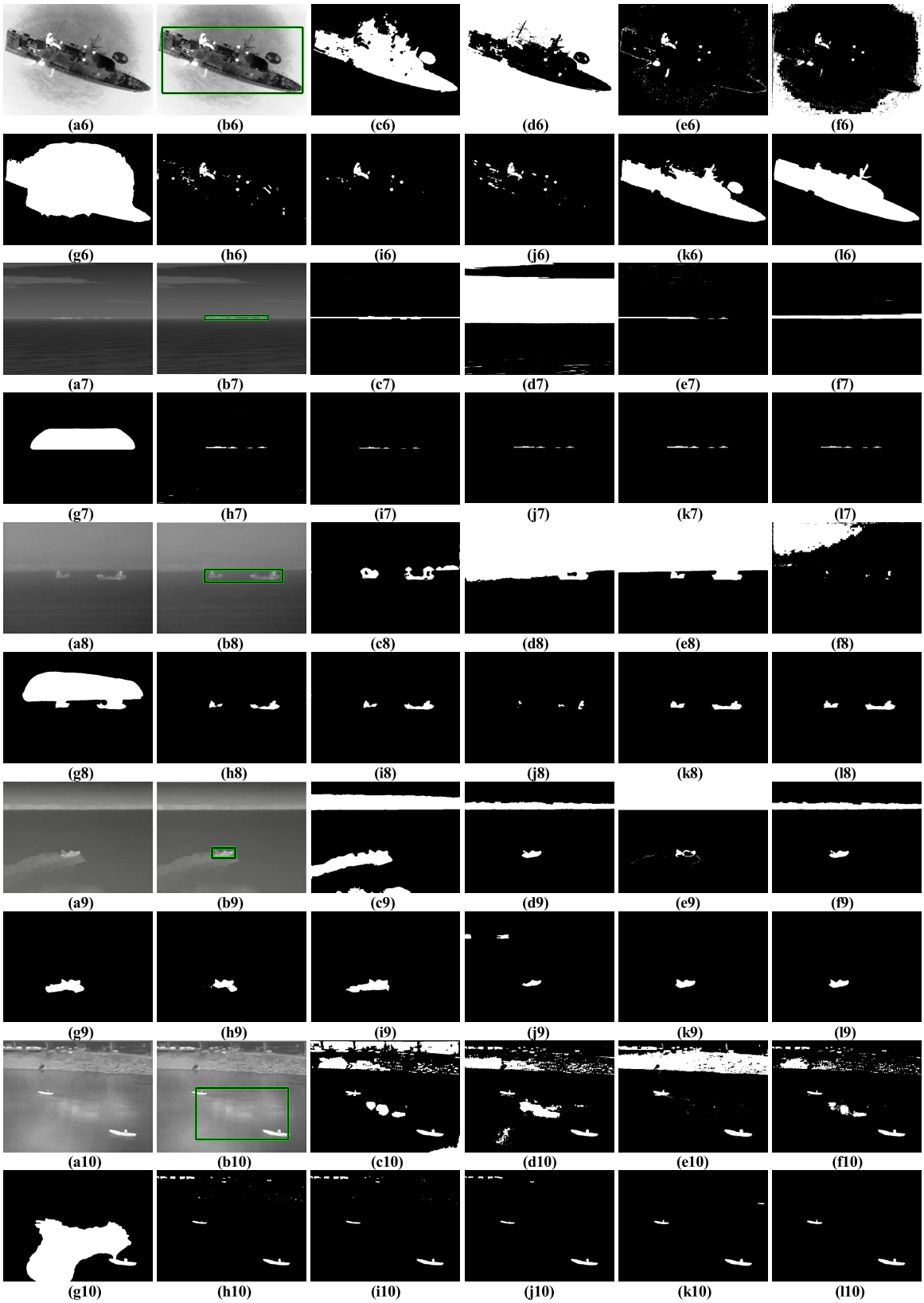

FIGURE 13. *(Continued.)* Segmentation results of different methods for the Figure 11. (a) The original IR ship images; (b) The initial curve (manually set) of the ECVM; (c)The segmentation results of WEMRF; (d) The segmentation results of 2DME; (e) The segmentation results of MSS; (f) The segmentation results of FCGCS; (g1-9) The segmentation results of ECVM; (h) The segmentation results of MFI; (i) The segmentation results of MRF-SFCM; (j) The segmentation results of MRMFA; (k) The segmentation results of the proposed method; (l) The ground-truth segmentation images (manually labeled).

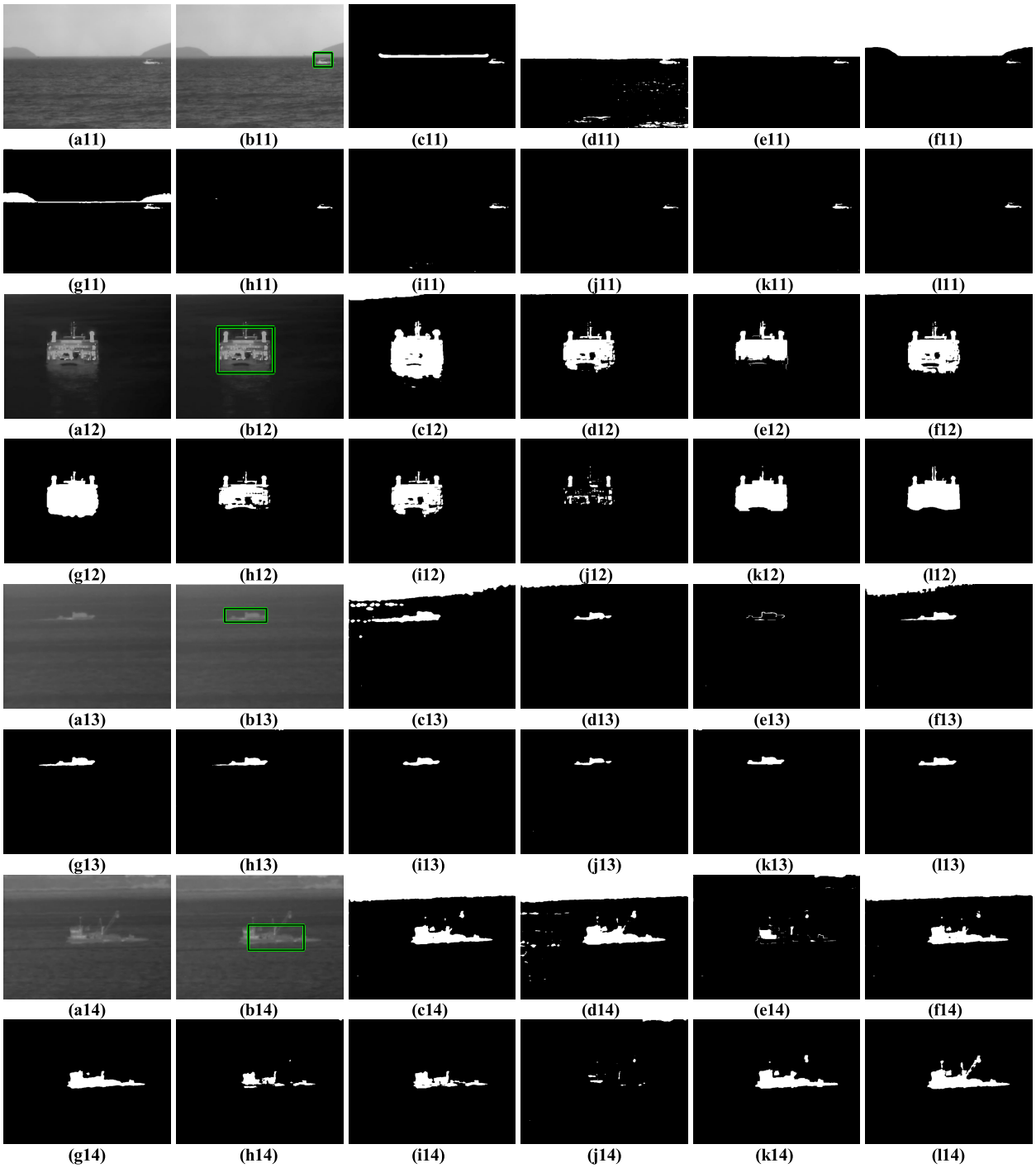

FIGURE 13. *(Continued.)* **Segmentation results of different methods for the Figure 11. (a) The original IR ship images; (b) The initial curve (manually set) of the ECVM; (c)The segmentation results of WEMRF; (d) The segmentation results of 2DME; (e) The segmentation results of MSS; (f) The segmentation results of FCGCS; (g1-9) The segmentation results of ECVM; (h) The segmentation results of MFI; (i) The segmentation results of MRF-SFCM; (j) The segmentation results of MRMFA; (k) The segmentation results of the proposed method; (l) The ground-truth segmentation images (manually labeled).**

the entire ship target. By combining above approaches and their advantages, the proposed method can effectively suppress the intricate background, and deal with the effects of the unknown brightness, uneven intensity, low contrast and variable size of ship target.

3) QUANTITATIVE COMPARISON TO IR SHIP TARGET SEGMENTATION BASELINE METHODS

To further evaluate the performance of IR ship target segmentation methods in the experiments, the misclassification error (ME) [1], [22] and the relative foreground area

TABLE 4. The segmentation performance of different methods for various IR ship images.

Metrics	Methods	WEMRF	2DME	MSS	FCGCS	ECVM	MFI	MRF-SFCM	MRMFA	The proposed
ME	Img.1	0.1082	0.0362	0.0410	0.2684	0.0008	0.0137	0.0162	0.0021	**0.0004**
	Img.2	0.0888	0.1673	0.0840	0.0797	0.0114	0.0019	0.0224	0.0073	**0.0009**
	Img.3	0.1663	0.2772	0.0300	0.1371	0.0009	0.0043	0.0010	0.0014	**0.0005**
	Img.4	0.0683	0.9619	0.0978	0.2685	0.0949	0.0866	0.0892	0.0894	**0.0134**
	Img.5	0.2417	0.6374	0.0391	0.1836	0.0647	0.0382	0.0355	0.0402	**0.0103**
	Img.6	0.0773	0.9555	0.2164	0.3969	0.2560	0.2053	0.2063	0.2022	**0.0310**
	Img.7	0.0137	0.4257	0.0063	0.0310	0.1158	0.0009	**0.0003**	**0.0003**	0.0008
	Img.8	0.0186	0.4784	0.4429	0.1393	0.1775	0.0056	0.0046	0.0121	**0.0035**
	Img.9	0.1919	0.0522	0.2579	0.0563	0.0130	0.0035	0.0122	0.0065	**0.0007**
	Img.10	0.1367	0.0886	0.1716	0.0423	0.2338	0.0059	0.0052	0.0035	**0.0019**
	Img.11	0.0151	0.4514	0.4218	0.3977	0.0259	**0.0003**	**0.0003**	0.0007	0.0006
	Img.12	0.0501	0.0155	0.0189	0.0214	0.0188	0.0198	0.0156	0.0562	**0.0042**
	Img.13	0.1080	0.0072	0.0075	0.0332	0.0021	0.0011	0.0010	0.0031	**0.0009**
	Img.14	0.1915	0.2034	0.0367	0.1899	0.0119	0.0255	0.0188	0.0409	**0.0068**
	Average	0.1054	0.3399	0.1337	0.1604	0.0734	0.0295	0.0306	0.0333	**0.0054**
RAE	Img.1	0.3386	0.9072	0.0752	0.3979	0.2104	0.2511	0.3917	0.3696	**0.0250**
	Img.2	0.7612	0.8398	0.5808	0.7490	0.5206	0.1181	0.6799	0.6892	**0.0043**
	Img.3	0.1444	0.0285	0.0826	0.3063	0.1524	0.1108	0.0986	0.2557	**0.0249**
	Img.4	0.2302	0.6834	0.8679	0.8992	0.4683	0.8715	0.9116	0.9181	**0.0608**
	Img.5	0.1937	0.7639	0.8115	0.9483	0.4708	0.8284	0.7364	0.8773	**0.0147**
	Img.6	0.1652	0.8810	0.9597	0.9700	0.5413	0.9364	0.9604	0.9410	**0.0577**
	Img.7	0.7857	0.9812	0.5702	0.8734	0.9777	0.0988	0.0380	**0.0136**	0.1014
	Img.8	0.2763	0.9496	0.9546	0.8757	0.9131	0.2445	0.1556	0.7846	**0.0393**
	Img.9	0.8801	0.1901	0.3650	0.1582	0.6547	0.3308	0.6413	0.3757	**0.0811**
	Img.10	0.1338	0.1039	0.2685	0.0435	0.9019	0.1163	0.1392	0.1254	**0.0069**
	Img.11	0.1415	0.9699	0.1627	0.4090	0.2865	0.0902	**0.0535**	0.1247	0.1180
	Img.12	0.3301	0.0546	0.1712	0.1067	0.1668	0.2724	0.0672	0.7809	**0.0162**
	Img.13	0.5246	0.2093	0.7818	0.0923	0.1945	0.0965	0.0863	0.3555	**0.0217**
	Img.14	0.1055	**0.0856**	0.7887	0.1638	0.2832	0.6029	0.4462	0.9265	0.1045
	Average	0.3579	0.5463	0.5315	0.4995	0.4816	0.3549	0.3861	0.5384	**0.0483**

error (RAE) [1], [22] are utilized as quantitative evaluation metrics. The ME denotes the percentage of pixels that are wrongly classified, that is, the background misclassified as foreground and the foreground misclassified as background. The RAE represents the segmented target area accuracy between the segmented image and the ground-truth image (manually labeled). Hence, the smaller ME and RAE imply the better results, and defined as:

$$ME = 1 - \frac{|B_O \cap B_T| + |F_O \cap F_T|}{|B_O| + |F_O|} \tag{26}$$

$$RAE = \begin{cases} \frac{A_O - A_T}{A_O}, & A_T < A_O \\ \frac{A_T - A_O}{A_T}, & A_T \geq A_O \end{cases} \tag{27}$$

where B_O and F_O are the background pixels and ship target pixels in the ground-truth image (manually labeled), respectively. B_T and F_T are the background pixels and ship target pixels of segmented image, respectively. $|\bullet|$ represents the cardinality of a set. A_O is the area of true target (manually labeled), and A_T is the area of segmented ship target. The ME and RAE values of different methods for various images are listed in Table 4, and the average ME and RAE values of each method on test dataset are listed in the second and third row of Table 5, respectively. Table 4 and Table 5 show that the proposed method obtains smaller average values for ME and RAE on all 14 IR ship images and test dataset than other compared eight methods, which implies that the proposed method has fewer misclassified pixels, and the ship target segmented by the proposed method is the closest to the ideal segmentation result in all methods. Consequently, the experimental results verify that the proposed method not only has better IR ship target segmentation capability compared with other classical and state-of-the-art methods, but also can work stably for different complex maritime scenarios.

TABLE 5. Quantitative evaluation of each method on test dataset.

Methods	WEMRF	2DME	MSS	FCGCS	ECVM	MFI	MRF-SFCM	MRMFA	The proposed
ME	0.1146	0.2433	0.1513	0.1537	0.0640	0.0141	0.0148	0.0207	**0.0038**
RAE	0.4340	0.5693	0.5423	0.4469	0.5210	0.2923	0.3114	0.5767	**0.0549**
Time(s)	19.9037	0.5175	4.9671	1.3897	26.8742	1.3445	1.1917	3.0330	0.8929

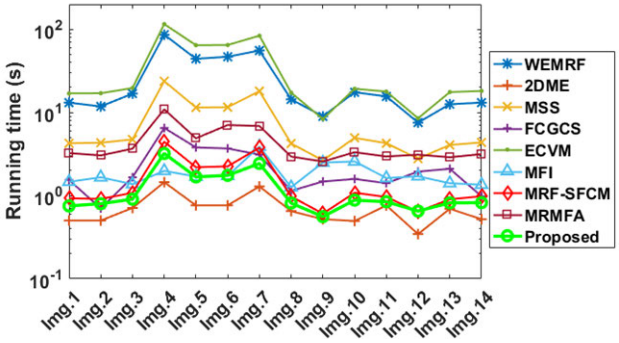

FIGURE 14. Running times of different methods for various IR ship images.

In order to analyze the time complexity of the proposed method, we counted the running times of different methods for various IR ship images, as shown in Fig. 14, and computed the average running time of each method on test dataset, as listed in the fourth row of Table 5. For better visual scale comparison, the vertical coordinate in Fig. 14 is the running time represented by logarithmic coordinate. It can be seen that the proposed method costs more time than 2DME method, but it is faster than other compared state-of-the-art methods. The reason is that the proposed method is based on the structure tensor, the maximum histogram entropy, and the new Watershed transform constructed by the ROI, which require less computation time. Therefore, through parallel computation and well-designed hardware, it can be easily implemented to real-time applications. To conclude, the proposed method not only outperforms the state-of-the-art methods in IR ship target segmentation but also is computationally economical.

VIII. CONCLUSION

In this paper, a new ship target segmentation method based on structure tensor and MHE is presented according to the intrinsic IR imaging properties between ship target and background clutter. The proposed method can automatically segment the ship target from diverse background clutters. By transforming the IR image into the STLE map, the horizon line and ship target boundary can be explicitly depicted. According to the scene context clue of IR ship images, the AHLD is proposed to judge whether the horizon line exists and locate the horizon line, so the sky or land region clutters can be reliably removed. Based on the intensity distribution of ship target and sea background, the AMHE is presented to accurately perceive the brightness (dark or bright) of ship target, thus the bright or dark IR ship target can be automatically segmented from sea background. The EGMR filter is designed to smooth heavy noise and fluctuating sea clutters while driving the brightness and intensity of ship target to be more consistent, so the ship target boundary information can be more reliably exploited to refine the IR ship target segmentation. Considering the ship target boundary information, the ROI of ship target can be accurately located by using edge strength-based image patch selection method, thus the SFM can be developed to solve the under-segmentation. Finally, the modified Watershed algorithm namely TEWT is constructed by fully integrating the advantages of the structure tensor and MHE, so the entire ship target can be completely extracted. Extensive experiments verify that the proposed algorithm has better IR ship segmentation performance than compared state-of-the-art methods, including WEMRF, 2DME, MSS, FCGCS, CVM, MFI, MRF-SFCM, and MRMFA. The experimental results also demonstrate that the proposed method can work stably for ship target with unknown brightness, uneven intensities, low contrast, variable quantities, sizes, and shapes with reasonable computational burden.

ACKNOWLEDGMENT

The authors would like to thank the relevant researchers for providing the image datasets. They are also grateful to express their thanks to anonymous reviewers for their insightful and valuable suggestions, which helped them to improve the quality of this paper.

REFERENCES

[1] X. Bai, Z. Chen, Y. Zhang, Z. Liu, and Y. Lu, "Infrared ship target segmentation based on spatial information improved FCM," *IEEE Trans. Cybern.*, vol. 46, no. 12, pp. 3259–3271, Dec. 2016.
[2] L. Dong, B. Wang, M. Zhao, and W. Xu, "Robust infrared maritime target detection based on visual attention and spatiotemporal filtering," *IEEE Trans. Geosci. Remote Sens.*, vol. 55, no. 5, pp. 3037–3050, May 2017.
[3] D. K. Prasad, D. Rajan, L. Rachmawati, E. Rajabally, and C. Quek, "Video processing from electro-optical sensors for object detection and tracking in a maritime environment: A survey," *IEEE Trans. Intell. Transp. Syst.*, vol. 18, no. 8, pp. 1993–2016, Aug. 2017.
[4] B. Wang, L. Dong, M. Zhao, H. Wu, Y. Ji, and W. Xu, "An infrared maritime target detection algorithm applicable to heavy sea fog," *Infr. Phys. Technol.*, vol. 71, pp. 56–62, Jul. 2015.
[5] M. Rodriguez-Blanco and V. Golikov, "Multiframe GLRT-based adaptive detection of multipixel targets on a sea surface," *IEEE J. Sel. Topics Appl. Earth Observ. Remote Sens.*, vol. 9, no. 12, pp. 5506–5512, Dec. 2016.
[6] Z. Liu, X. Bai, C. Sun, F. Zhou, and Y. Li, "Multi-modal ship target image smoothing based on adaptive mean shift," *IEEE Access*, vol. 6, pp. 12573–12586, 2018.
[7] Y. Li, X. Mao, D. Feng, and Y. Zhang, "Fast and accuracy extraction of infrared target based on Markov random field," *Signal Process.*, vol. 91, no. 5, pp. 1216–1223, May 2011.
[8] H. Wang, Z. Zou, Z. Shi, and B. Li, "Detecting ship targets in spaceborne infrared image based on modeling radiation anomalies," *Infr. Phys. Technol.*, vol. 85, pp. 141–146, Sep. 2017.

[9] A. Zhou, W. Xie, and J. Pei, "Infrared maritime target detection using the high order statistic filtering in fractional Fourier domain," *Infr. Phys. Technol.*, vol. 91, pp. 123–136, Jun. 2018.
[10] Z. Tian-Xu, Z. Guang-Zhou, W. Fei, and Z. G. Xi, "Fast recursive algorithm for infrared ship image segmentation," *J. Infr. Millim. Waves*, vol. 25, no. 4, p. 295, 2006.
[11] D. Feng, S. Wenkang, C. Liangzhou, D. Yong, and Z. Zhenfu, "Infrared image segmentation with 2-D maximum entropy method based on particle swarm optimization (PSO)," *Pattern Recognit. Lett.*, vol. 26, no. 5, pp. 597–603, Apr. 2005.
[12] C. W. Park, "Extracting targets from regions-of-interest in infrared images using a 2-D histogram," *Opt. Eng.*, vol. 50, no. 2, Feb. 2011, Art. no. 027003.
[13] X. Wang, "Clutter-adaptive infrared small target detection in infrared maritime scenarios," *Opt. Eng.*, vol. 50, no. 6, Jun. 2011, Art. no. 067001.
[14] J. Wu, "Ship target detection and tracking in cluttered infrared imagery," *Opt. Eng.*, vol. 50, no. 5, May 2011, Art. no. 057207.
[15] B. Wang, L. Dong, M. Zhao, and W. Xu, "Fast infrared maritime target detection: Binarization via histogram curve transformation," *Infr. Phys. Technol.*, vol. 83, pp. 32–44, Jun. 2017.
[16] S. Yin, C. Kong, Y. Wang, and W. Wang, "Effective infrared ship image segmentation using fuzzy correlation and graph cut optimization," *J. Electron. Imag.*, vol. 27, no. 04, p. 1, Aug. 2018.
[17] Z. L. Szpak and J. R. Tapamo, "Maritime surveillance: Tracking ships inside a dynamic background using a fast level-set," *Expert Syst. Appl.*, vol. 38, no. 6, pp. 6669–6680, Jun. 2011.
[18] D. Frost and J.-R. Tapamo, "Detection and tracking of moving objects in a maritime environment using level set with shape priors," *EURASIP J. Image Video Process.*, vol. 2013, no. 1, p. 42, Jul. 2013.
[19] L. Fang, X. Wang, and Y. Wan, "Adaptable active contour model with applications to infrared ship target segmentation," *J. Electron. Imag.*, vol. 25, no. 4, Jun. 2016, Art. no. 041010.
[20] L. Fang, W. Zhao, X. Li, and X. Wang, "A convex active contour model driven by local entropy energy with applications to infrared ship target segmentation," *Opt. Laser Technol.*, vol. 96, pp. 166–175, Nov. 2017.
[21] W. Tao, "Unified mean shift segmentation and graph region merging algorithm for infrared ship target segmentation," *Opt. Eng.*, vol. 46, no. 12, Dec. 2007, Art. no. 127002.
[22] Z. Liu, F. Zhou, X. Chen, X. Bai, and C. Sun, "Iterative infrared ship target segmentation based on multiple features," *Pattern Recognit.*, vol. 47, no. 9, pp. 2839–2852, Sep. 2014.
[23] Z. Liu, X. Bai, C. Sun, F. Zhou, and Y. Li, "Infrared ship target segmentation through integration of multiple feature maps," *Image Vis. Comput.*, vols. 48–49, pp. 14–25, Apr. 2016.
[24] X. Bai, Z. Chen, Y. Zhang, Z. Liu, and Y. Lu, "Spatial information based FCM for infrared ship target segmentation," in *Proc. IEEE Int. Conf. Image Process. (ICIP)*, Oct. 2014, pp. 5127–5131.
[25] X. Bai, M. Liu, T. Wang, Z. Chen, P. Wang, and Y. Zhang, "Feature based fuzzy inference system for segmentation of low-contrast infrared ship images," *Appl. Soft Comput.*, vol. 46, pp. 128–142, Sep. 2016.
[26] Y. Li, Z. Li, Y. Zhu, B. Li, W. Xiong, and Y. Huang, "Thermal infrared small ship detection in sea clutter based on morphological reconstruction and multi-feature analysis," *Appl. Sci.*, vol. 9, no. 18, p. 3786, Sep. 2019.
[27] S. He, X. Wang, R. Xia, W. Jin, and J. Liang, "Polarimetric infrared imaging simulation of a synthetic sea surface with Mie scattering," *Appl. Opt.*, vol. 57, no. 7, pp. B150–B159, Feb. 2018.
[28] U. Köthe, "Edge and junction detection with an improved structure tensor," in *Proc. Joint Pattern Recognit. Symp.* Berlin, Germany: Springer, 2003, pp. 25–32.
[29] A. V. Kanaev, W. Hou, S. R. Restaino, S. Matt, and S. Gladysz, "Restoration of images degraded by underwater turbulence using structure tensor oriented image quality (STOIQ) metric," *Opt. Express*, vol. 23, no. 13, p. 17077, Jun. 2015.
[30] D. Liu, L. Cao, Z. Li, T. Liu, and P. Che, "Infrared small target detection based on flux density and direction diversity in gradient vector field," *IEEE J. Sel. Topics Appl. Earth Observ. Remote Sens.*, vol. 11, no. 7, pp. 2528–2554, Jul. 2018.
[31] L. Liu, F. Liang, J. Zheng, D. He, and J. Huang, "Ship infrared image edge detection based on an improved adaptive canny algorithm," *Int. J. Distrib. Sensor Netw.*, vol. 14, no. 3, Mar. 2018, Art. no. 155014771876463.
[32] S. Kim and J. Lee, "Small infrared target detection by region-adaptive clutter rejection for sea-based infrared search and track," *Sensors*, vol. 14, no. 7, pp. 13210–13242, Jul. 2014.
[33] L. A. F. Fernandes and M. M. Oliveira, "Real-time line detection through an improved Hough transform voting scheme," *Pattern Recognit.*, vol. 41, no. 1, pp. 299–314, Jan. 2008.
[34] Z. Cui, J. Yang, S. Jiang, J. Li, L. Lin, and Y. Gu, "An infrared-small-target detection method in compressed sensing domain based on local segment contrast measure," *Infr. Phys. Technol.*, vol. 93, pp. 41–52, Sep. 2018.
[35] P. L. Rosin, "Unimodal thresholding," *Pattern Recognit.*, vol. 34, no. 11, pp. 2083–2096, Nov. 2001.
[36] X.-C. Yuan, L.-S. Wu, and Q. Peng, "An improved OTSU method using the weighted object variance for defect detection," *Appl. Surf. Sci.*, vol. 349, pp. 472–484, Sep. 2015.
[37] Q. Li and S. Ren, "A visual detection system for rail surface defects," *IEEE Trans. Syst., Man, Cybern. C, Appl. Rev.*, vol. 42, no. 6, pp. 1531–1542, Nov. 2012.
[38] J. N. Kapur, P. K. Sahoo, and A. K. C. Wong, "A new method for gray-level picture thresholding using the entropy of the histogram," *Comput. Vis., Graph., Image Process.*, vol. 29, no. 1, pp. 273–285, Jan. 1985.
[39] L. Vincent, "Morphological grayscale reconstruction in image analysis: Applications and efficient algorithms," *IEEE Trans. Image Process.*, vol. 2, no. 2, pp. 176–201, Apr. 1993.
[40] J.-J. Chen, C.-R. Su, W. E. L. Grimson, J.-L. Liu, and D.-H. Shiue, "Object segmentation of database images by dual multiscale morphological reconstructions and retrieval applications," *IEEE Trans. Image Process.*, vol. 21, no. 2, pp. 828–843, Feb. 2012.
[41] C. Gao, D. Meng, Y. Yang, Y. Wang, X. Zhou, and A. G. Hauptmann, "Infrared patch-image model for small target detection in a single image," *IEEE Trans. Image Process.*, vol. 22, no. 12, pp. 4996–5009, Dec. 2013.
[42] Y. Li, Z. Li, K. Wei, W. Xiong, J. Yu, and B. Qi, "Noise estimation for image sensor based on local entropy and median absolute deviation," *Sensors*, vol. 19, no. 2, p. 339, Jan. 2019.
[43] X. Liu, M. Tanaka, and M. Okutomi, "Single-image noise level estimation for blind denoising," *IEEE Trans. Image Process.*, vol. 22, no. 12, pp. 5226–5237, Dec. 2013.
[44] L. Dong, J. Zhou, and Y. Y. Tang, "Effective and fast estimation for image sensor noise via constrained weighted least squares," *IEEE Trans. Image Process.*, vol. 27, no. 6, pp. 2715–2730, Jun. 2018.
[45] J. M. Gauch, "Image segmentation and analysis via multiscale gradient watershed hierarchies," *IEEE Trans. Image Process.*, vol. 8, no. 1, pp. 69–79, Jan. 1999.
[46] R. Gaetano, G. Masi, G. Poggi, L. Verdoliva, and G. Scarpa, "Marker-controlled watershed-based segmentation of multiresolution remote sensing images," *IEEE Trans. Geosci. Remote Sens.*, vol. 53, no. 6, pp. 2987–3004, Jun. 2015.
[47] M. Ciecholewski, "River channel segmentation in polarimetric SAR images: Watershed transform combined with average contrast maximisation," *Expert Syst. Appl.*, vol. 82, pp. 196–215, Oct. 2017.
[48] L. Vincent and P. Soille, "Watersheds in digital spaces: An efficient algorithm based on immersion simulations," *IEEE Trans. Pattern Anal. Mach. Intell.*, vol. 13, no. 6, pp. 583–598, Jun. 1991.
[49] D. D. Bloisi, L. Iocchi, A. Pennisi, and L. Tombolini, "ARGOS-venice boat classification," in *Proc. 12th IEEE Int. Conf. Adv. Video Signal Based Surveill. (AVSS)*, Aug. 2015, pp. 1–6.
[50] L. Patino, T. Cane, A. Vallee, and J. Ferryman, "PETS 2016: Dataset and challenge," in *Proc. IEEE Conf. Comput. Vis. Pattern Recognit. Workshops (CVPRW)*, Jun. 2016, pp. 1240–1247.
[51] *Al Salam Boccaccio 98 Images*. Accessed: Jun. 16, 2019. [Online]. Available: https://commons.wikimedia.org/wiki/Category:Al_Salam_Boccaccio_98_(ship,_1970)
[52] N. Otsu, "A threshold selection method from gray-level histograms," *IEEE Trans. Syst., Man, Cybern.*, vol. SMC-9, no. 1, pp. 62–66, Jan. 1979.

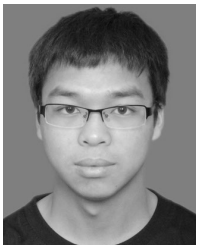

YONGSONG LI received the B.S. degree in electronic information science and technology from Zhengzhou University, Zhengzhou, China. He is currently pursuing the Ph.D. degree with the School of Microelectronics and Communication Engineering, Chongqing University, Chongqing, China. His current research interests include infrared image processing, noise estimation, pattern recognition, and remote sensing.

ZHENGZHOU LI received the B.S. degree from Northeastern University, Shenyang, China, in 1998, and the M.S. degree in physics electronics and the Ph.D. degree in optical engineering from the Institute of Optics and Electronics, Chinese Academy of Sciences, Chengdu, China, in 2001 and 2004, respectively. He was a Postdoctoral Fellow with the Department of Ophthalmology, Harvard Medical School, USA. He is currently a Professor with Chongqing University and with the Institute of Optics and Electronics, Chinese Academy of Sciences, China. His research interests include target detection and tracking, and image and signal processing for remote sensing.

ZHIQUAN DING received the B.S. degree in information material and the M.S. degree in signal and information processing from the University of Electronic Science and Technology of China, Chengdu, China, in 1998 and in 2007, respectively. He is a Senior Engineer with the Sichuan Institute of Aerospace Electronic Equipment and with the Research and Development Center of Intelligent Detection and Recognition Technology of MultiSensor, Chengdu. His research interests include target detection and tracking, and signal processing and information fusion.

TIANQI QIN received the B.S. degree in mathematics and applied mathematics (pure) and the Ph.D. degree in mathematics in uncertainty processing from Sichuan University, Chengdu, China, in 2011 and 2016, respectively. She is currently an Engineer with the Sichuan Institute of Aerospace Electronic Equipment and with the Research and Development Center of Intelligent Detection and Recognition Technology of MultiSensor, Chengdu. Her research interests include target detection and tracking, signal processing, and information fusion.

WEIQI XIONG received the B.S. degree in electronic information engineering from Chongqing University, Chongqing, China, where he is currently pursuing the M.S. degree in electronics and communication engineering. His current research interests include signal processing and pattern recognition.